Dimethyl itaconate induces long-term innate immune responses and confers protection against infection

Ferreira, A.V.; Kostidis, S.; Groh, L.A.; Koeken, V.A.C.M.; Bruno, M.; Baydemir, I.; ... ; Domínguez-Andrés, J.

Cell Reports

Article

Dimethyl itaconate induces long-term innate immune responses and confers protection against infection

Anaísa V. Ferreira,[1,2,*] Sarantos Kostidis,[3] Laszlo A. Groh,[1] Valerie A.C.M. Koeken,[1,4,5] Mariolina Bruno,[1]
Ilayda Baydemir,[1] Gizem Kilic,[1] Özlem Bulut,[1] Theano Andriopoulou,[6] Victoria Spanou,[6] Kalliopi D. Synodinou,[6]
Theologia Gkavogianni,[6] Simone J.C.F.M. Moorlag,[1] L. Charlotte de Bree,[1] Vera P. Mourits,[1] Vasiliki Matzaraki,[1]
Werner J.H. Koopman,[7] Frank L. van de Veerdonk,[1] Georgios Renieris,[6] Martin Giera,[3]
Evangelos J. Giamarellos-Bourboulis,[6] Boris Novakovic,[8,9] and Jorge Domínguez-Andrés[1,10,*]

[1]Department of Internal Medicine and Radboud Center for Infectious Diseases, Radboud University Nijmegen Medical Centre, 6500HB Nijmegen, the Netherlands
[2]Instituto de Ciências Biomédicas Abel Salazar (ICBAS), Universidade do Porto, 4050-313 Porto, Portugal
[3]Center for Proteomics and Metabolomics, Leiden University Medical Center, 2333ZA Leiden, the Netherlands
[4]TWINCORE, a Joint Venture Between the Helmholtz-Centre for Infection Research (HZI) and the Hannover Medical School (MHH), 30625 Hannover, Germany
[5]Centre for Individualised Infection Medicine (CiiM), Department of Computational Biology for Individualised Infection Medicine, a Joint Venture Between the Helmholtz-Centre for Infection Research (HZI) and the Hannover Medical School (MHH), 30625 Hannover, Germany
[6]4th Department of Internal Medicine, National and Kapodistrian University of Athens, Medical School, Athens, Greece
[7]Department of Pediatrics, Amalia Children's Hospital, Radboud Center for Mitochondrial Medicine, Radboud University Medical Center, Nijmegen, the Netherlands
[8]Murdoch Children's Research Institute, Parkville, VIC 3052, Australia
[9]Department of Paediatrics, University of Melbourne, Parkville, VIC 3052, Australia
[10]Lead contact
*Correspondence: anaisa.validoferreira@radboudumc.nl (A.V.F.), jorge.dominguezandres@radboudumc.nl (J.D.-A.)
https://doi.org/10.1016/j.celrep.2023.112658

SUMMARY

Itaconate is an immunomodulatory metabolite produced by immune cells under microbial stimulation and certain pro-inflammatory conditions and triggers antioxidant and anti-inflammatory responses. We show that dimethyl itaconate, a derivative of itaconate previously linked to suppression of inflammation and widely employed as an alternative to the endogenous metabolite, can induce long-term transcriptional, epigenomic, and metabolic changes, characteristic of trained immunity. Dimethyl itaconate alters glycolytic and mitochondrial energetic metabolism, ultimately leading to increased responsiveness to microbial ligand stimulation. Subsequently, mice treated with dimethyl itaconate present increased survival to infection with *Staphylococcus aureus*. Additionally, itaconate levels in human plasma correlate with enhanced *ex vivo* pro-inflammatory cytokine production. Collectively, these findings demonstrate that dimethyl itaconate displays short-term anti-inflammatory characteristics and the capacity to induce long-term trained immunity. This pro-and anti-inflammatory dichotomy of dimethyl itaconate is likely to induce complex immune responses and should be contemplated when considering itaconate derivatives in a therapeutic context.

INTRODUCTION

Itaconate (ITA) is an intriguing metabolite that has been recently explored for its broad immunomodulatory properties in mammalian systems. Under pro-inflammatory conditions, activated immune cells increase the expression of the immune-responsive gene 1 (IRG1) enzyme, which decarboxylates the Krebs cycle intermediate *cis*-aconitate to ITA.[1] Upregulating ITA concentrations is an important metabolic feedback on inflammation.[2,3] The transcription factor NRF2 is activated by dimethyl ITA (DMI), leading to the induction of antioxidant responses and a decrease in the expression of pro-inflammatory genes.[4] ITA also acts as a competitive succinate dehydrogenase (SDH) inhibitor, blocking the progression of the Krebs cycle from succi-

nate to fumarate. Impairment of SDH, or complex II of the electron transport chain (ETC), compromises succinate oxidation and thus the transfer of electrons to the ubiquinone pool.[2] ITA also inhibits the glycolytic enzyme fructose-6-phosphate 2-kinase,[5] while the derivative 4-octyl ITA (OI) inhibits glyceraldehyde-3-phosphate dehydrogenase and thereby blocks the increased glycolysis in pro-inflammatory macrophages.[6] The immunosuppressive and antioxidant effects of ITA and its derivatives DMI and OI have been described in various disease models, such as cardiac ischemia-reperfusion injury, psoriasis, and infection. In *in vivo* mouse models, DMI reduces myocardial infarct size[2] and prevents the scaling and skin edema typically seen in psoriasis,[4] and mice that lack *IRG1* show increased susceptibility to *Mycobacterium tuberculosis* infection due to

enhanced pathological inflammatory responses.[7] Besides these anti-inflammatory properties, ITA also presents direct antimicrobial activity by inhibiting isocitrate lyase, an enzyme found in different pathogenic microorganisms such as *M. tuberculosis*, *Candida albicans*, or *Staphylococcus aureus*[1,8,9] In particular, DMI treatment ameliorated *S. aureus* ocular infection in mice.[10] However, in other models, *S. aureus* and *P. aeruginosa* have also adapted to ITA-rich environments by using it as a carbon source for the production of biofilms, which are associated with chronic infections of these microorganisms.[11,12] These properties make ITA and its derivatives one of the most promising group of molecules with therapeutic potential in pathologies characterized by exacerbated inflammatory responses.[13]

The anti-inflammatory properties of DMI have also been reported in trained immunity,[14] the phenomenon where the innate immune system can exhibit an increased responsiveness to a second unrelated stimulus following an earlier immune insult, also known as innate immune memory.[15] In this regard, treatment with DMI is able to impair the induction of trained immunity in human monocytes stimulated with β-glucan, a cell-wall component of *C. albicans*.[14]

These previous studies investigated the effects of ITA and its derivatives in an established inflammatory context. In this work, however, we demonstrate that the anti-inflammatory effects of DMI are context dependent and that DMI, in the absence of other stimuli, is able to trigger enhanced responsiveness against heterologous secondary stimuli, thus highlighting the dual role of DMI as a molecule with anti-inflammatory and immune potentiating characteristics.

RESULTS

ITA and its derivatives increase the responsiveness of human monocytes to secondary stimulation

In order to explore the possible role of ITA and its derivatives as inducers of long-term inflammatory responses, we used an established *in vitro* model of trained immunity.[16] Human peripheral blood monocytes were exposed to ITA, OI, or DMI for 24 h and left to differentiate for the following 5 days in the absence of any stimulus, after which the differentiated macrophages were restimulated with the TLR4 agonist lipopolysaccharide (LPS) for 24 h (Figure 1A). Contrary to the previously described anti-inflammatory characteristics of ITA, exposure to ITA led to increased production of interleukin-6 (IL-6), and OI treatment led to enhanced tumor necrosis factor α (TNF-α) secretion, both upon restimulation (Figures 1B and 1C). DMI-exposed macrophages (DMI-Mfs) showed increased TNF-α and IL-6 secretion after LPS restimulation, in a similar magnitude as the well-described inducer of trained immunity β-glucan (Figure 1D, left panels). DMI-Mfs also showed enhanced TNF-α and IL-6 production upon TLR2 activation with the agonist Pam₃Cys (P3C) (Figure 1D, right panels). This pro-inflammatory feature of DMI was not observed after acute stimulation. Monocytes exposed to DMI for 24 h did not produce detectable levels of the pro-inflammatory cytokines IL-1β, TNF-α, and IL-6, while the secretion of the anti-inflammatory cytokine IL-10 was reduced and IL-1Ra was increased (Figure S1A). In accordance with the described acute anti-inflammatory properties of DMI, DMI decreased

monocytes' phagocytic capacity (Figure S1B); however, DMI had no effect on monocyte fungal killing capacity (Figure S1C).

DMI induces epigenomic modulation in human monocytes

The long-term responsive phenotype in trained cells is supported by epigenomic reprogramming.[17–21] Accordingly, DMI-Mfs exhibited enriched deposition of the histone 3 trimethylation of lysine 4 (H3K4me3) mark and decreased deposition of the H3K9me3 mark at the promoter regions of *TNFA* and *IL6* (Figure 1E). These epigenomic alterations suggest poised transcription of the *TNFA* and *IL6* genes and decreased heterochromatin in these regions. The relevance of epigenomic changes is further supported by the decreased responsiveness of cells exposed to the protein methylation inhibitor methylthioadenosine (MTA) (Figure 1F). Here, we demonstrated that DMI leads to epigenomic modulation akin to the changes elicited by the prototypical inducers of trained immunity.

DMI triggers a similar transcriptional signature to β-glucan and modulates interferon responses

Previous costimulation experiments showed that DMI decreased LPS-derived inflammation[4] and blunted β-glucan-derived trained immunity[14]; however, we now report that DMI exposure alone triggers trained immunity. To dissect these two profiles of DMI, we performed a transcriptomic study of *in vitro* monocytes (Figure 2A). Firstly, the transcription signatures of β-glucan- and DMI-exposed monocytes were both distinct from non-trained control samples at day 1 (Figure 2B). Functional enrichment analysis of upregulated and downregulated genes demonstrated that the top enriched pathways were similar between DMI- and β-glucan-exposed cells (Figures S2A and S2B). Of note, although we have previously reported that DMI inhibited β-glucan trained immunity,[14] the transcriptional response triggered by the combined exposure of DMI and β-glucan was largely similar to the individual DMI or β-glucan treatment (Figures 2B, S2A, and S2B). However, there were specific differences in the early (4 h) monocyte response to DMI+ β-glucan compared with β-glucan alone (Figures 2C–2E), namely that the presence of DMI blocked the β-glucan-driven increase of genes from the "Toll-like receptor," "TNF," and "nuclear factor κB (NF-κB)" signaling pathways while enhancing genes in the "sphingolipid metabolism" pathway (Figure 2E).

Secondly, DMI has been described as an anti-inflammatory metabolite, mainly in monocyte LPS costimulation experiments, while we observed that DMI exposure alone led to differentiation of trained macrophages. Thus, we sought to determine if these two opposing early and long-term effects shared a transcriptional signature. DMI enhanced and attenuated specific LPS-induced genes, both in monocytes after 4 h stimulation and in DMI-trained macrophages stimulated for 4 h with LPS at day 6 (Figure 2F). In monocytes, promoter motif analysis of the group of genes enhanced by DMI+LPS when compared with LPS alone revealed that the activating transcription factor 3 (ATF3) promoter motif signature was enriched (Figure S2C, top panel). Accordingly, ATF3 protein levels were shown to rise after DMI exposure.[4] Interestingly, the DMI-attenuated LPS response gene set in monocytes (Figure 2F, left panel) and the DMI-trained
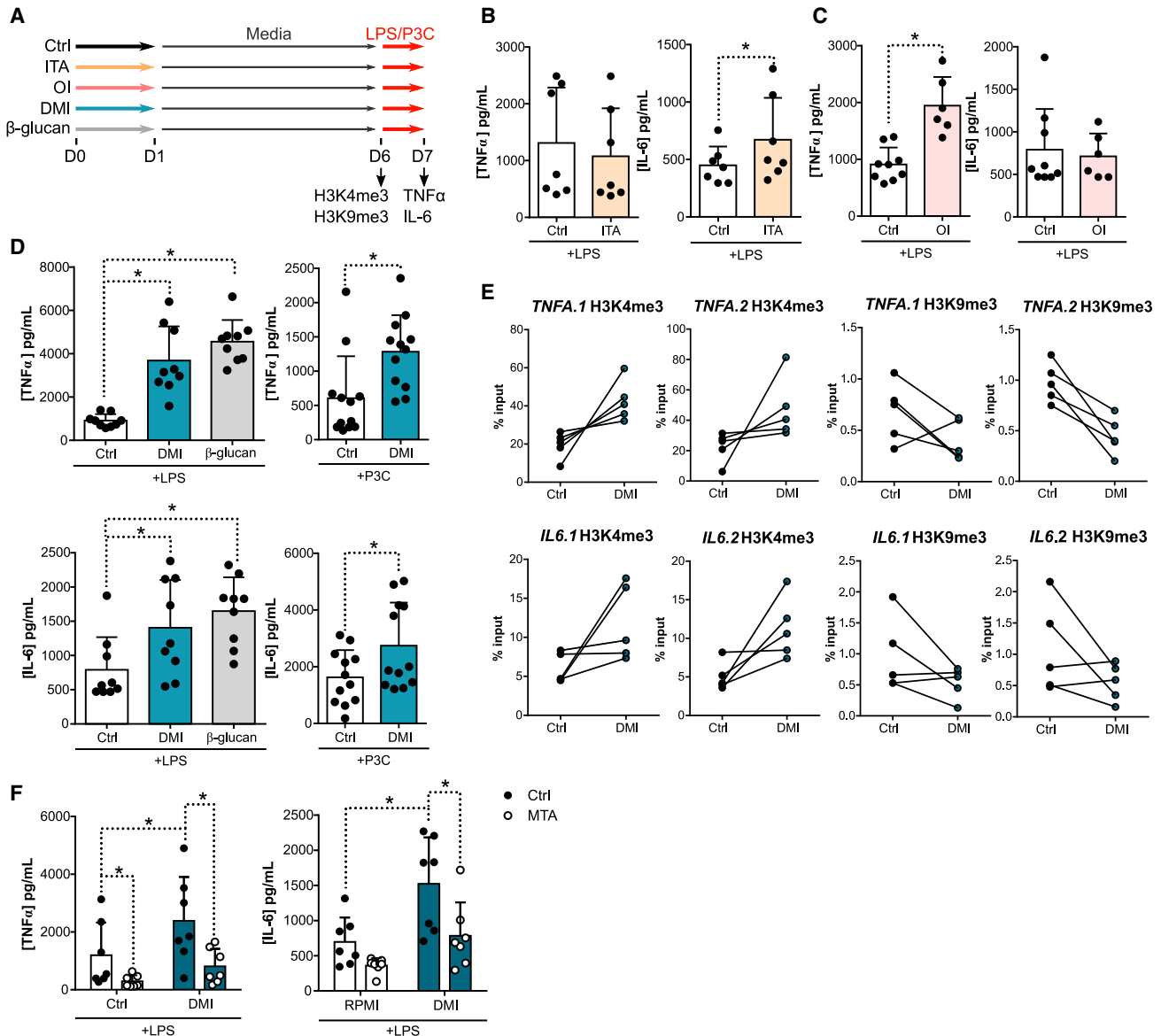
Figure 1. DMI increases TNF-α and IL-6 production upon restimulation

(A) Schematic depiction of the *in vitro* trained immunity protocol.

(B and C) TNF-α and IL-6 production by peripheral blood monocytes exposed to 5 mM itaconate (ITA) or 100 μM 4-octyl itaconate (OI) for 24 h and restimulated with 10 ng/mL LPS 6 days later for another 24 h (n = 6–7 pooled from 2 independent experiments).

(D) TNF-α and IL-6 production by monocytes treated with 250 μM dimethyl itaconate (DMI) and stimulated 6 days later with 10 ng/mL LPS or 10 μg/mL Pam3Cys (P3C) for another 24 h (n = 9/12 pooled from 3/4 independent experiments).
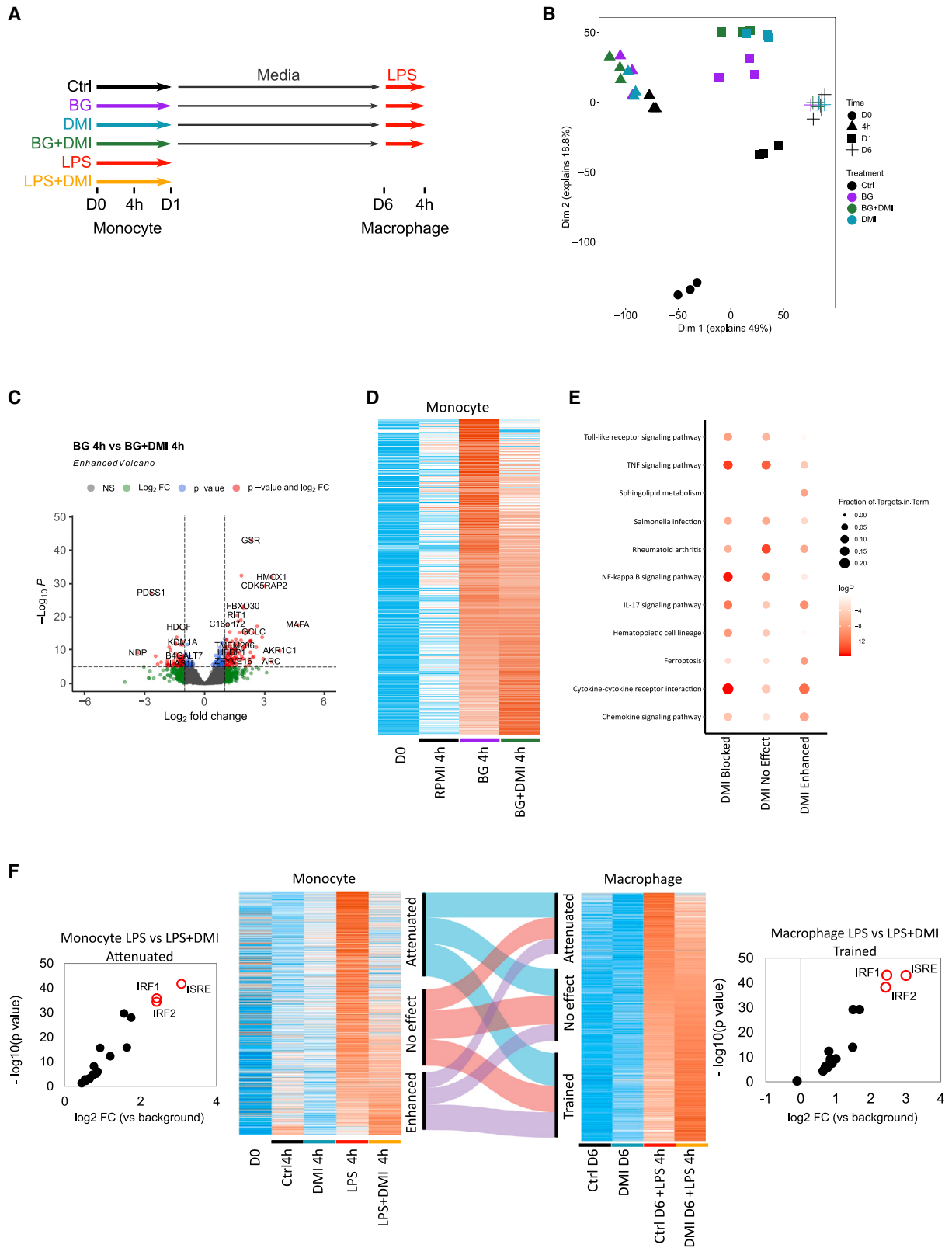
(E) Deposition of H3K4me3 and H3K9me3 marks at two promoter sites (.1 and .2) of *TNFA* and *IL6* of DMI-exposed monocytes at 6 days of culture (n = 5 pooled from 2 independent experiments).

(F) TNF-α and IL-6 production by monocytes treated with 0.5 mM MTA and 250 μM DMI for 24 h and restimulated with 10 ng/mL LPS at day 6 of culture for another 24 h (n = 7, pooled from 2 independent experiments).

Mean + SD, *p < 0.05, Wilcoxon signed-rank test; (F) two-way ANOVA, Sidak's multiple comparisons test.

gene set in macrophage LPS response (Figure 2F, right panel) were both enriched for the interferon (IFN)-stimulated response element (ISRE) and the IFN regulatory factors 1 and 2 (IRF1/2). ISRE enrichment is also seen in the gene group attenuated in DMI-Mfs (Figure S2C, bottom panel). Similar to DMI-Mfs, the genes attenuated and trained in β-glucan-Mfs were also enriched for ISRE and IRF motifs (Figures S2D and S2E). Collectively, these data support that DMI induced transcriptional changes comparable to those triggered by the trained immunity inducer β-glucan.

A

B

C

BG 4h vs BG+DMI 4h
EnhancedVolcano

D

Monocyte

E

F

Monocyte LPS vs LPS+DMI
Attenuated

Monocyte

Macrophage

Macrophage LPS vs LPS+DMI
Trained

(legend on next page)

DMI stimulates glycolytic and mitochondrial energy metabolic rates

Cellular metabolism shares a reciprocal link with epigenomic and transcriptional landscapes.[22] Using a trained immunity *in vitro* model, we found that DMI-Mfs displayed decreased intracellular glucose, increased glucose consumption (Figure 3A), elevated lactate secretion (Figure 3B), and increased basal and maximal extracellular acidification rate (ECAR) (Figure 3C), all indicative of a high glycolytic rate. In addition, DMI-Mfs displayed an increased basal oxygen consumption rate (OCR) (Figure 3D), suggesting higher oxidative respiration. DMI-Mfs exhibited slightly higher concentrations of the TCA cycle metabolites succinate, fumarate, and malate. At the same time, pyruvate and glutamine were decreased (Figure 3E). The upregulation of glycolysis was observed starting from 24 h of DMI exposure (Figure S3A), but the OCR was not enhanced (Figure S3B). TCA cycle metabolites citrate and malate were significantly increased in DMI-exposed monocytes (Figure S3C). After LPS restimulation, DMI-Mfs still had lower glucose intracellular concentrations, higher levels of lactate release, and a tendency for decreased intracellular pyruvate (Figures S3D and S3E), highlighting that DMI upregulated glycolysis in a persistent and long-term manner.

The parallel increase in glycolysis and oxidative phosphorylation suggests that DMI treatment increases both the glycolytic and mitochondrial metabolic rate in macrophages. This is supported by the fact that DMI-Mfs displayed higher ATP content (Figure 3F, top panel). To determine the relative contribution of mitochondria to the total ATP production, the activity of mitochondrial ATP-producing synthase (F_oF_1-ATPase) was prevented using oligomycin. This inhibition reduced ATP content in both control and DMI-Mf, and the relative contribution of glycolysis and mitochondria to the total ATP level was similar between groups (Figure 3F, bottom panel). The contribution of F_oF_1-ATPase activity to DMI-Mf responsiveness is observed by the decreased production of IL-6 by cells stimulated with LPS and oligomycin (Figure 3G). Glycolysis upregulation also contributed to DMI-Mf responsiveness, as seen by the decrease of TNF-α and IL-6 production, due to the inhibition of intracellular glucose uptake by 2-DG (Figure 3H).

These metabolic changes, indicative of high glycolytic and mitochondrial metabolism, were exclusive to DMI and β-glucan since they were not observed in ITA-exposed cells (Figures S4A–S4D). In contrast, ITA induced succinate accumulation (Figure S4B), which aligns with the previously described SDH inhibition.[23] However, ITA-Mfs resolved the accumulated succinate, while intracellular fumarate and glutamate content was decreased (Figure S4D). Regarding DMI inhibition of β-glucan-induced trained immunity, similar to what we observed transcriptionally, DMI did not strongly alter the general metabolic profile of β-glucan-exposed cells (Figures S4E and S4F). DMI weakly potentiated the ECAR and OCR of β-glucan-exposed monocytes (Figure S4G) and reduced H3K9me3 deposition at the promoter region of *TNFA* (Figure S4H).

DMI induces mitochondrial perturbations in human monocytes

Mitochondrial metabolism and ATP production strongly contribute to trained immunity, so we set out to explore different parameters of mitochondrial function. Firstly, we assessed reactive oxygen species (ROS) levels by quantifying the oxidation of a mitochondria-targeted hydroethidium (HEt) variant (MitoSOX). Monocytes exposed to DMI for 24 h displayed increased HEt oxidation, indicative of increased levels of HEt-oxidizing ROS (Figure 4A, left panel). However, the DMI-induced increase in HEt oxidation was transient, since DMI-Mfs displayed a slight decrease in HEt oxidation (Figure 4A, right panel). Human macrophages trained with oxidized low-density lipoprotein showed increased HEt oxidation, and the mitochondria-targeted antioxidant MitoTempo (MT) decreased the augmented pro-inflammatory cytokines produced by these cells.[24] However, pre-treatment with MT did not decrease DMI-enhanced cytokine production (Figure 4B). To further access mitochondrial function, we used TMRE. This fluorescent cation accumulates in the mitochondrial matrix across the mitochondrial inner membrane (MIM) in a manner dependent on the *trans*-MIM mitochondrial membrane potential ($\Delta\psi$). To determine the minimal TMRE fluorescence signal, $\Delta\psi$ was dissipated using the mitochondrial uncoupler FCCP (Figure 4C). Following normalization of the TMRE signals on the FCCP-treated condition, no effect of acute DMI treatment was observed (Figure 4D, left panel). In contrast, the TMRE signal was increased in macrophages previously exposed to DMI and β-glucan (Figure 4D, right panel), suggesting a more negative (hyperpolarized) $\Delta\psi$. Similarly, time-lapse analysis of TMRE fluorescence demonstrated a significantly higher signal in DMI-treated vs. control cells (Figure 4E). Acute inhibition of the mitochondrial F_oF_1-ATPase (i.e., OXPHOS complex V) by oligomycin significantly increased TMRE fluorescence in DMI-Mfs and apparently increased this signal in control cells (Figure 4E). These results, combined with the fact that oligomycin inhibited the OCR in control and DMI-Mfs (see Figure 3D, bottom panel), strongly suggest that the F_oF_1-ATPase operates in its forward (ATP-producing) mode under our experimental conditions. This supports the conclusion that the ETC is more active after the

---

Figure 2. DMI exposure induces a long-term transcriptional signature associated with interferon responses

(A) Experimental model including the collection time points of 0, 4 h, day 1, day 6, and day 6+4 h and the respective stimuli (n = 3).

(B) Principal-component analysis (PCA) plot based on transcriptional changes (7,217 genes) associated with 2 μg/mL β-glucan, 250 μM DMI, and β-glucan+DMI treatments at day 0, 4 h, day 1, and day 6 time points.

(C and D) Enhanced volcano plot (C) and heatmap (D) of differentially expressed genes in response to 4 h stimulation with β-glucan or β-glucan+DMI.

(E) Bubble map of the functional enrichment analysis at 4 h of genes being transcriptionally attenuated, not changed, or enhanced in β-glucan+DMI-treated monocytes when compared with β-glucan-treated cells.

(F) Heatmaps and Sankey plot of differentially expressed genes by monocytes in response to 250 μM DMI, 1 ng/mL LPS, or LPS+DMI after 4 h stimulation or by macrophages trained with DMI and restimulated with 10 ng/mL LPS for 4 h, and scatterplot of −log10 (p value) and log2 fold change of the abundance of a transcription factor binding motif relative to background occurrence. Motifs were analyzed in the genes identified regarding monocytes (left) and macrophages (right) at 4 h and 6 days+4 h time points, respectively.
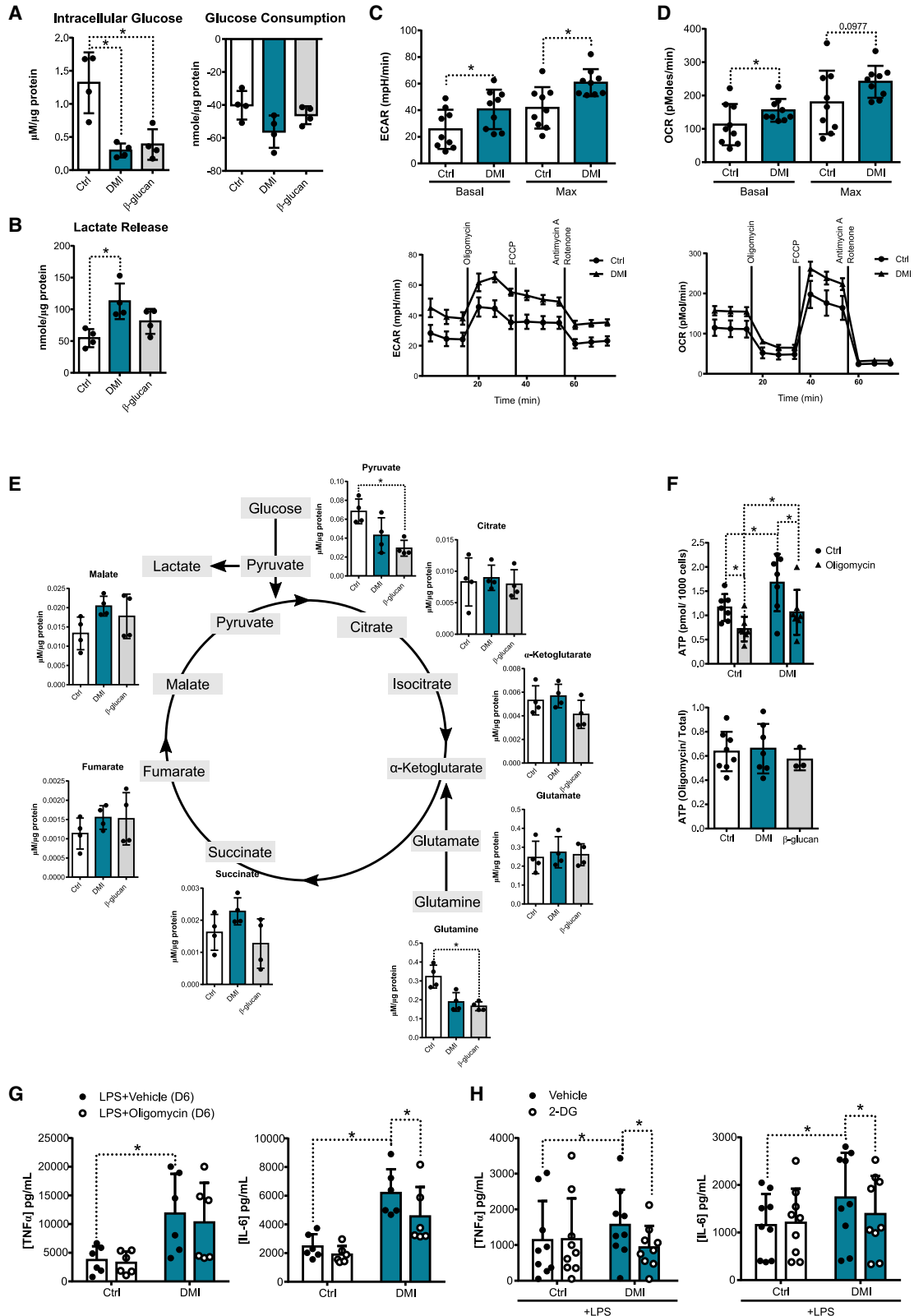
(legend on next page)

5 day resting period, allowing the F_oF_1-ATPase to actively contribute to the increase in cellular ATP content in DMI-Mfs.

DMI increases general ROS levels in human monocytes

ITA is characterized not only by its anti-inflammatory features but also by the activation of the antioxidant response via Nrf2 activation.[4] As previously reported, the expression of the Nrf2 target genes *NQO1* and *HMOX1* and ROS detoxifying enzymes *SOD* and *CAT* were upregulated in DMI-exposed monocytes (Figure 4F). However, this was not observed in ITA-exposed cells (Figure 4G). Also, monocytes exposed to DMI prior to stimulation with zymosan had decreased chemiluminescence due to luminol oxidation when compared with zymosan-activated cells, indicative of lower general (gen)ROS levels (Figure 4H). However, monocytes that were exposed to DMI alone, in the absence of other stimuli, showed increased oxidation of the ROS species indicator H_2DCFDA compared with control cells, which pointed to higher basal genROS levels in DMI-treated cells. Increased H_2DCFDA oxidation was present not only after acute DMI stimulation of 2 and 24 h but also after the resting period of 5 days (Figure 4I). To determine if ROS contributed to the induction of increased responsiveness in DMI-Mfs, we performed genetic and pharmacological approaches. Patients with chronic granulomatous disease (CGD) are characterized by a failure to mount a respiratory burst due to mutations in genes of the NADPH oxidase (NOX) complex.[25] Trained macrophages derived from patients with CGD produced lower amounts of TNF-α and IL-6 after LPS restimulation compared with healthy controls (Figure 4J). However, the decreased responsiveness is not specific to DMI-Mfs since control cells from patients with CGD also responded less when compared with healthy controls (Figure 4J). To clarify the role of NOX in DMI trained immunity, we pharmacologically inhibited NOX activity with diphenyleneiodonium (DPI) and found no differences in TNF-α and IL-6 secretion after restimulation of DMI-Mfs (Figure 4K). On the other hand, genROS scavenger molecules N-acetyl cysteine (NAC) and α-tocopherol (AT) significantly modulated the responsiveness to LPS in DMI-Mfs (Figure 4L). AT further enhanced TNF-α and IL-6 production in DMI-Mfs, but it also increased IL-6 secretion in control cells. In contrast, NAC decreased TNF-α production. Collectively, we showed that DMI triggered the antioxidant response when combined with other stimulants, as previously described. However, when DMI was used in isolation, genROS levels were sustainably increased, reflecting the highly energetic metabolism of DMI-Mfs.

Glutathione metabolism plays a role in DMI-induced responsiveness

The DMI-induced high energy metabolism and ROS increase could be linked to a modified cellular redox status. Thus, we hypothesized that glutathione (GSH) might play a role in DMI-induced trained immunity. The expression of glutamate-cysteine ligase catalytic (*GCLC*) subunit and glutathione reductase (*GSR*) were upregulated after 5 h DMI exposure, pointing to an increase in synthesis and reduction of GSH, respectively (Figure 5A). The expression of the thiol antioxidant thioredoxin (*TXN*) and reducing enzyme *TXNDR1* were also increased (Figure 5A). This upregulation was not observed in cells stimulated with ITA for 4 h (Figure 5B). GSH intracellular levels were decreased in monocytes exposed to DMI for 5 h (Figure 5C), and inhibition of the GSH-synthesizing enzyme γ-glutamyl cysteine ligase (GCL) by buthionine sulphoximine (BSO) further decreased GSH levels (Figure 5C). In contrast, monocytes treated for 24 h (Figure 5D, left panel), DMI-Mfs (Figure 5E, left panel), and restimulated DMI-Mfs (Figure S5A) show increased GSH concentrations when compared with control cells. Similarly, oxidized glutathione levels (GSSG) were also enhanced after 24 h DMI treatment (Figure 5D, middle panel), while in contrast, GSSG was decreased in DMI-Mfs (Figure 5D, middle panel). Thus, we observed that the increase of the intracellular glutathione pool was triggered by acute DMI exposure and sustained at 6 days of culture (Figures 5C and 5D, left panels). Of note, the GSH-to-GSSG ratio was not increased after acute DMI exposure (Figure 5F), but for DMI-Mfs, the ratio was enhanced (Figure 5G). The electron cycler nicotinamide adenine dinucleotide (NAD) was also increased at the three time points (Figures 5H, 5I, and S5A). Collectively, these data point to an increase in GSH synthesis and recycling in DMI- and β-glucan-exposed cells (Figures 5D–5G).

After 24 h, this increase in GSH content was not accompanied by significant general consumption of upstream metabolites (Figures 5K and 5L) except for a decrease in the intracellular content of glycine (Figure 5K). On the other hand, DMI-Mfs had less intracellular methionine, serine, and glycine (Figure 5M) and consumed more cystine from the media (Figure 5N). Serine, cystine, and glycine were also increasingly consumed upon LPS restimulation by DMI-Mfs when compared with non-trained cells (Figures S5B and S5C). Thus, we have observed that the upregulation of the glutathione synthesis pathway was common between DMI and the trained immunity-inducer β-glucan, while ITA did not have a similar effect (Figures 5D and 5E). The

---

Figure 3. DMI promotes a long-term change in glycolysis, oxidative phosphorylation, TCA cycle, and ATP concentration

(A and B) Intracellular glucose, glucose consumption (A), and (B) lactate release of 250 μM DMI-Mf and 2 μg/mL β-glucan-Mf at day 6 of culture (n = 4).

(C and D) Basal and maximum (Max) extracellular acidification rate (ECAR) (C) and oxygen consumption rate (OCR) (D) of DMI-Mf was also determined 5 days after 24 h stimulation with DMI by extracellular flux measurements (n = 9 pooled from 3 independent experiments).

(E) Concentration of different TCA cycle intermediates present in DMI-Mfs and β-glucan-Mfs after 6 days of culture (n = 4).

(F) ATP concentration of DMI-Mfs and 1 μg/mL β-glucan-Mf. Prior to the collection at day 6, half the cells were exposed to 1 μM oligomycin for 30 min (n = 3/7 pooled from 2/3 independent experiments).

(G) TNF-α and IL-6 production by human monocytes treated with 250 μM DMI for 24 h and restimulated with 10 ng/mL LPS and 1 μM oligomycin 5 days later (n = 6 pooled from 2 independent experiments).

(H) TNF-α and IL-6 production by human monocytes treated with 250 μM DMI and 1 mM 2-DG for 24 h and restimulated with 10 ng/mL LPS (n = 9 pooled from 3 independent experiments).

Mean ± SD, *p < 0.05; (A, B, and E) one-way ANOVA, Dunnett's multiple comparisons test; (C and D) Wilcoxon signed-rank test; (F–H) two-way ANOVA, Sidak's multiple comparisons test.
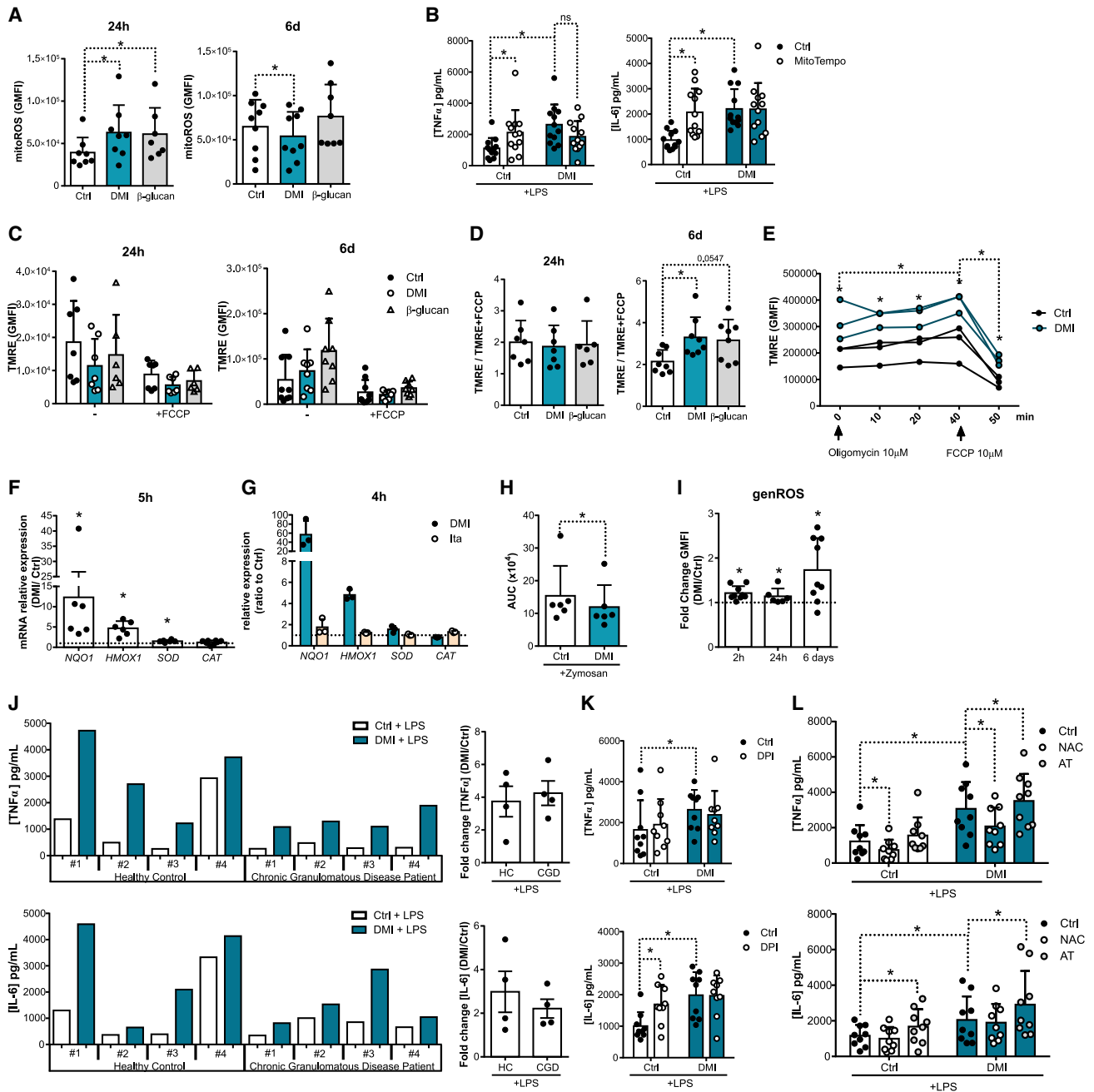
Figure 4. DMI modulates reactive oxygen species (ROS) production

(A) Mitochondrial ROS levels (MitoSox) in monocytes exposed to DMI or 1 μg/mL β-glucan-Mf for 24 h and at 6 days of culture (n = 7–9 pooled from 4 independent experiments).

(B) TNF-α and IL-6 production by monocytes pre-treated with 500 μM MitoTempo (MT) exposed to DMI for 24 h and restimulated with 10 ng/mL LPS after 5 days for 24 h (n = 12 pooled from 4 independent experiments or n = 3 from 1 experiment, respectively).

(C) Mitochondrial membrane potential was accessed by TMRE staining in the presence or absence of 10 μM FCCP.

(D) TMRE staining was normalized with TMRE staining of FCCP-treated cells (TMRE GMFI/TMRE TMRE [+FCCP] GMFI) (n = 5–7, pooled from 3 independent experiments).

(E) Cells pre-exposed to DMI were stained with TMRE at day 6 of culture. TMRE fluorescence was measured for 40 min after the addition of 10 μM oligomycin. 10 μM FCCP was added after 40 min and fluorescence measured after 10 min (n = 3, pooled from 3 independent experiments).

(F) Expression of genes of the antioxidant response *NQO1* (NAD(P)H:quinone oxidoreductase 1), *HMOX1* (heme oxygenase-1), *SOD* (superoxide dismutase), and *CAT* (catalase) in monocytes exposed to DMI for 5 h (n = 6 pooled from 2 independent experiments).

(G) Expression of *NQO1*, *HMOX1*, *SOD*, and *CAT* upon DMI or ITA exposure for 4 h.

(legend continued on next page)

contribution of the increased glutathione content to DMI-Mf responsiveness was observed by the dampened production of TNF-α and IL-6 by cells exposed to BSO, a glutathione synthase inhibitor, which was reversed by the concomitant addition of ethyl (Et)GSH (Figure 5O). However, the reduction in DMI-Mf responsiveness induced by BSO does not appear to be regulated by a decrease of H3K4me3 deposition at the promoter regions of *TNFA* and *IL6* genes (Figure S6). Collectively, these data suggest that DMI-induced trained immunity depended on a tightly balanced regulation of GSH concentration.

ITA and DMI associate with trained immunity *in vivo*

We next investigated the association of ITA and DMI with trained immunity features *in vivo*. Firstly, we explored the potential of DMI to induce protection against infection *in vivo* by using a mouse model of trained immunity. Mice received daily DMI injections for 4 days and/or were infected with a sublethal dose of *C. albicans*, which triggers a systemic induction of trained immunity in the animals.[26] After 7 days, mice were subjected to infection with the gram-positive bacteria *S. aureus*. (Figure 6A). In line with our *in vitro* findings, DMI administration led to an increased protection against an *S. aureus* challenge (Figure 6B). This result may reflect the ability of DMI to induce trained immunity *in vivo*, offering protection against heterologous infections. Also similar to what was demonstrated *in vitro*,[14] the protection conferred by *C. albicans* is ablated when mice are concomitantly exposed to DMI (Figure 6C). The effect of DMI on mice survival demonstrated that, when in the absence of another stimulation, DMI may exert immunostimulatory properties, while it shows anti-inflammatory characteristics when combined with a pro-inflammatory stimulus.

To further assess the functional relevance of our findings in humans, we analyzed a cohort of healthy volunteers vaccinated with BCG (300BCG cohort) (Figure 6D), where peripheral blood mononuclear cells were collected before and 14 and 90 days after BCG vaccination and stimulated *ex vivo* with *S. aureus* for 24 h and 7 days. We assessed whether common SNPs (minor allele frequency [MAF] > 0.05) in a window of 500 kb around *IRG1* were associated with changes in pro-inflammatory cytokine production. For this, we performed quantitative trait locus (QTL) mapping using genetic and cytokine data from the 300BCG cohort. We identified four SNPs suggestively associated ($p < 9.99 \times 10^{-3}$) with changes in IL-6 (rs9593198, p = 0.0087; rs7323290, p = 0.0013), IL-1β (rs606861, p = 0.0048), and IFNγ (rs7988715, p = 0.006) secretion (Figure 6E), potentially pointing to a role for IRG1 expression in the regulation BCG-enhanced cytokine production. Additionally, we evaluated the association between baseline circulating plasma ITA concentrations and the BCG-enhanced pro-inflammatory cytokine production upon *ex vivo* restimulation. ITA levels prior to vaccination were modestly associated with the fold change of

IL-1β (p = 0.028) and TNF-α (p = 0.016) production upon BCG vaccination (Figure 6F), suggesting that endogenous ITA levels may also potentiate the capacity of pro-inflammatory cytokine production.

DISCUSSION

In this study, we show that DMI is an inducer of trained immunity. The protection of DMI-injected mice against *S. aureus* infection supports the ability of DMI to enhance immune functions, while *in vitro* DMI-Mfs are transcriptionally similar to β-glucan-Mfs and likewise show increased pro-inflammatory cytokine production upon restimulation.

To date, the study of ITA and its derivatives has been mainly conducted in inflammatory contexts, where ITA molecules dampen the production of the enhanced pro-inflammatory mediators. In this study, we highlight a diametric outcome where DMI decreases LPS inflammatory responses while potentiating innate immune memory, specifically at the level of metabolism, ROS production, and production of pro-inflammatory cytokines upon secondary stimulation. To unravel this characteristic of DMI, we set out to determine if DMI could induce transcriptional signatures involved in both pro-and anti-inflammatory processes, and we identified one common response. In monocytes, the group of genes attenuated by DMI+LPS when compared with LPS alone were enriched for the ISRE and IRF1/2 promoter motif signature. Interestingly, these promoter motifs were also enriched in the DMI-trained gene set in the macrophage LPS response. This enrichment of IFN response-related motifs might be at the center of the dichotomic characteristic of DMI. Moreover, β-glucan-Mf differentially expressed genes were also enriched for IFN response-related motifs. IFN signaling has been shown to be required for trained immunity: IFNγ-receptor-deficient mice vaccinated with BCG failed to mount an innate immune memory response,[27] and *in vitro* monocytes trained with BCG while IFNγ production was blocked did not show enhanced cytokine production.[21] Thus, IFN responses could be a common player in the establishment of trained immunity.

DMI has also been shown to inhibit β-glucan-induced trained immunity *in vitro*.[14] Similarly, we show that DMI prevents the increase of survival conferred by *C. albicans*-induced trained immunity in a mouse model of infection. Although DMI inhibits β-glucan trained immunity *in vitro*, here, we have not observed that DMI induces metabolic changes consistent with a decrease in responsiveness of β-glucan-Mfs. However, DMI dampened the transcription of specific relevant functional pathways induced by β-glucan. Specifically, DMI blocks the upregulation of genes related to "Toll-like receptor signaling," "TNF," "NF-κB," and "cytokine-cytokine receptor interaction" pathways. The dampening of these signaling networks may account for

---

(H) ROS levels in monocytes pre-treated with DMI for 30 min and then stimulated with 1 mg/mL zymosan (n = 6 pooled from 2 independent experiments).

(I) Basal levels of ROS in monocytes exposed to DMI for 2 h, 24 h, or after 6 days of culture (n = 6–9 pooled from 2 to 3 independent experiments).

(J) TNF-α and IL-6 production by monocytes from healthy controls and patients with chronic granulomatous disease after treatment with DMI for 24 h followed by 10 ng/mL LPS restimulation at day 6 of culture for another 24h.

(K and L) TNF-α and IL-6 production by human monocytes pre-treated for 1 h with (K) 0.5 μM diphenyleneiodonium (DPI), (L) 50 μM α-tocopherol (AT), or 1 mM N-acetyl cysteine (NAC), exposed to DMI for 24 h, and restimulated with 10 ng/mL LPS after 5 days for 24 h. n = 9 pooled from 3 independent experiments. Mean ± SD, *p < 0.05; Wilcoxon signed-rank test; (B, E, K, and L) two-way ANOVA, Sidak's multiple comparisons test.
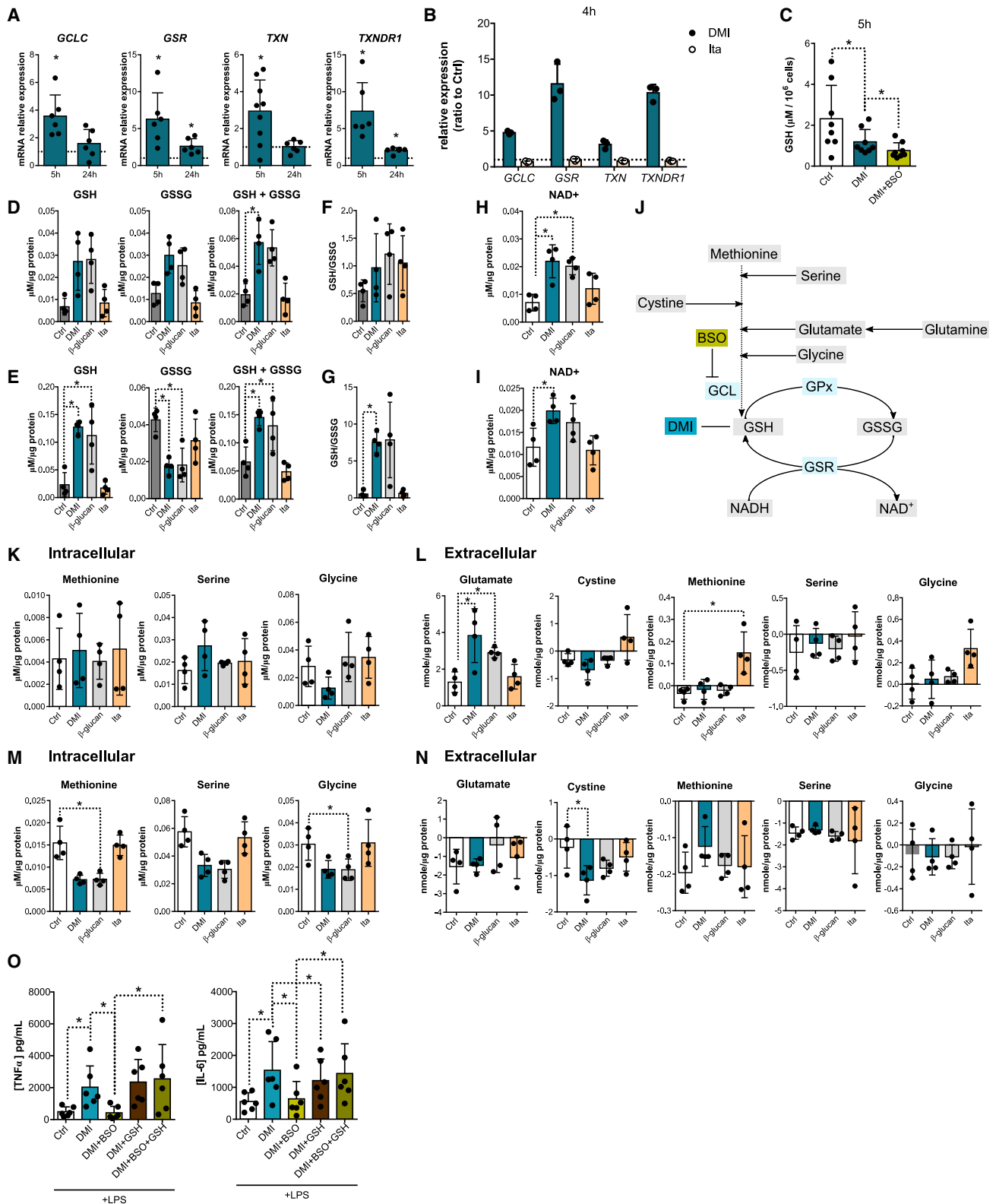
Figure 5. DMI-induced trained immunity depends on modulation of glutathione

(A) Expression of *GCLC* (γ-glutamyl cysteine ligase catalytic subunit), *GSR* (glutathione-disulfide reductase), *TXN* (thioredoxin), and *TXNRD1* (thioredoxin reductase 1) in monocytes exposed to 250 μM DMI for 5 and 24 h (n = 6–9 pooled from 2 to 3 independent experiments).

(legend continued on next page)

the inhibitory effect of DMI on β-glucan-induced trained immunity.

Previous studies have explored the acute metabolic effects of ITA and derivatives on activated myeloid cells. Upon LPS exposure, glycolysis was downregulated by ITA and derivatives.[3,6,28] In contrast, bone marrow-derived naive macrophages exposed to DMI exhibit an increase in glycolysis.[2] Considering that other inducers of trained immunity trigger changes in metabolic and epigenomic networks that support macrophage effector functions, we investigated whether DMI could also lead to such an epigenomic and metabolic reprogramming. Indeed, we show that a short DMI exposure induces a long-term metabolic rewiring characterized by increased glycolytic and mitochondrial ATP generation, which was necessary for the increased DMI-Mf responsiveness. These findings are in accordance with the profile of β-glucan- or BCG-trained monocytes, in which inhibition of glycolysis ablates β-glucan trained immunity,[18] and genetic variation in genes of the ETC are associated with changes in BCG trained immunity traits.[29] The potentiation of mitochondrial ATP generation by DMI was accompanied by changes in mitochondrial ROS levels and a hyperpolarized *trans*-MIM potential, suggesting that DMI enhanced ETC activity.

In addition to increased mitochondrial-derived ROS levels, we also observed that DMI exposed cells generally displayed higher basal levels of ROS. In the case of β-glucan- and BCG-trained macrophages, ROS levels were also increased, and antioxidant response genes were upregulated.[30,31] In contrast, when activated, DMI decreased ROS generation. Although ITA and its derivates have been attributed antioxidant characteristics, they have been shown to induce oxidative stress in some contexts. Namely, LPS-tolerized RAW264.7 cells that overexpress *IRG1* present higher levels of genROS than the tolerized control cell line, while *IRG1* silencing decreased genROS levels in the same model.[32] *IRG1* overexpression in the human monocytic cell line THP-1 led to an increase in genROS levels,[33] and the mouse microglia cell line BV2 exposed to DMI had an enhanced genROS production as well.[4] Also, in a zebrafish model of infection with *Salmonella enterica*, *IRG1* depletion in macrophage-lineage cells decreased HEt oxidation and compromised bactericidal activity.[34] Compatible with these results, a study on a zebrafish model of gouty inflammation demonstrated that *IRG1* depletion decreased macrophage-specific HEt oxidation.[35] The potential effect of DMI-induced ROS generation in the modulation of macrophage effector functions, such as phagocytosis and microbicidal activity, remains to be explored. However, through antioxidant pharmacological approaches, we have observed that the increase in genROS and mitochondrial-derived ROS does not play a crucial role in DMI-Mf responsiveness. Of note, the opposing effects of NAC and AT on cytokine production may be due to these molecules' distinct scavenging properties. NAC is not only an effective antioxidant molecule but also acts as a precursor of glutathione, the main endogenous antioxidant molecule, while AT is present in lipid structures and inhibits lipid peroxidation, preventing damage of membranes.[36]

The alteration in ROS levels could not only be indicative of a highly active cellular metabolism but could also suggest a change in the capacity for ROS scavenging. GSH is the most abundant thiol that scavenges ROS and protects against oxidative stress. DMI reacts with thiols and can form conjugates with GSH, decreasing its intracellular levels while increasing ROS.[4,37] Also, variations in genes involved in the glutathione pathway have been shown to modulate β-glucan- and BCG-induced trained immunity traits,[30] and bone marrow-derived macrophages isolated from β-glucan-trained mice have increased levels of glutathione.[31] Indeed, here, we have observed that acute DMI exposure quickly decreased GSH cellular levels and concomitantly increased GSH synthesis and recycling, which led to a long-term GSH enrichment of DMI-Mfs. The increase of GSH synthesis was also observed for β-glucan-Mfs, while ITA did not modulate GSH levels. The upregulation of GSH synthesis was necessary for DMI-Mf responsiveness, highlighting the crucial role of GSH metabolism in DMI-induced trained immunity.

Epigenetic changes modulate transcription and contribute for trained immunity responsiveness.[38,39] Here, we observed that epigenomic marks on the promoter regions of pro-inflammatory cytokine genes, *TNFA* and *IL6*, are altered in DMI-Mfs, which potentially contributes to increased secretion of these cytokines upon DMI-Mf stimulation. However, there are other layers of epigenomic regulation that would be interesting to explore in a DMI trained immunity setting in future studies, such as the possibility of itaconylation of histone lysine residues as a post-translational modification similar to acetylation or succinylation[3,28] or the direct binding of GSH to histones, a process termed glutathionylation.[40]

In addition to the immunopotentiation characteristic of DMI, we show that plasma ITA levels were associated with higher cytokine responses in a BCG trained immunity human cohort. ITA concentrations have previously been correlated with a reduction in rheumatoid arthritis disease progression,[41] and patients with idiopathic pulmonary fibrosis have reduced concentrations of ITA in the lungs.[42] Interestingly, the induction of

---

(B) *GCLC*, *GSR*, *TXN*, and *TXNDR1* expression of monocytes exposed to 250 μM DMI or 5 mM ITA for 4 h (n = 3).

(C) GSH levels in monocytes exposed to 250 μM DMI, 25 μM buthionine sulphoximine (BSO), or both for 5h (n = 8 pooled from 3 independent experiments).

(D–G) Concentration of glutathione (GSH, GSSG) (D–F) and nicotinamide adenine dinucleotide (NAD+) (H and I) after 24 h monocyte stimulation with 250 μM DMI, 2 μg/mL β-glucan, or 5 mM ITA (D, F, and H) and after 6 days of culture (E, G, and I) (n = 4).

(J) Schematic representation of glutathione metabolism (glutamate-cysteine ligase [GCL], glutathione peroxidase [GPx]).

(K and M) Intracellular levels of methionine, serine, and glycine in monocytes exposed to DMI, β-glucan, or ITA for (K) 24 h or (M) at day 6 of culture (n = 4).

(L and N) Consumption (values < 0) or release (values > 0) into the conditioned media of glutamate, cystine, methionine, serine, and glycine by monocytes exposed to DMI, β-glucan, or ITA for (L) 24 h or (N) at day 6 of culture (n = 4).

(O) TNF-α and IL-6 production by human monocytes pre-treated for 1 h with 25 μM BSO, 1 mM EtGSH, or a combination of 25 μM BSO and 1 mM EtGSH, exposed to DMI for 24 h, and restimulated with 10 ng/mL LPS after 5 days for 24 h (n = 6 pooled from 2 independent experiments).

Mean ± SD, *p < 0.05; (A–C) Wilcoxon signed-rank test; (D–I and K–N) one-way ANOVA, Dunnett's multiple comparisons test; (O) two-way ANOVA, Sidak's multiple comparisons test.
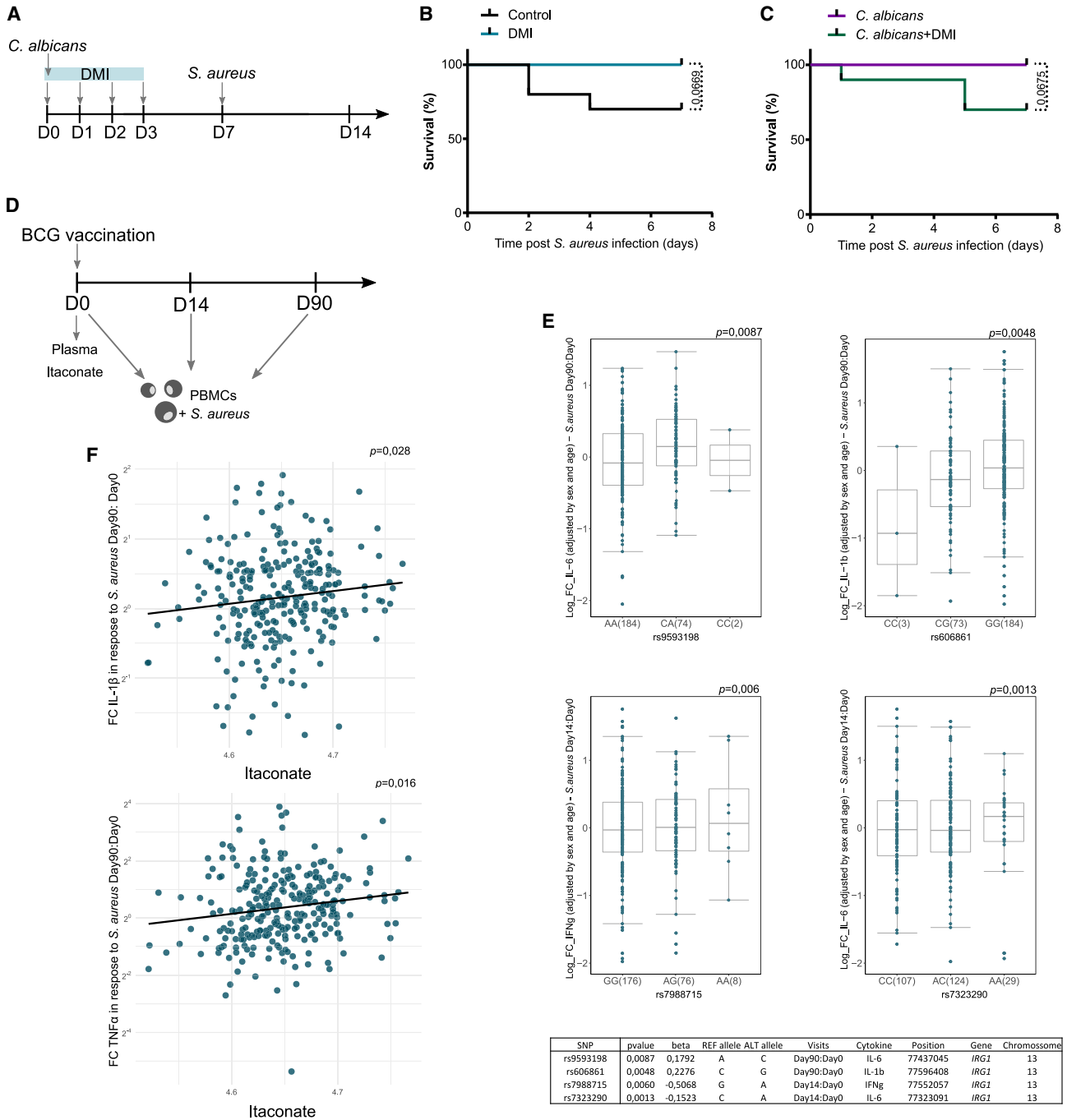
Figure 6. DMI and itaconate correlate with *in vivo* trained immunity features

(A) Graphic representation of the mouse survival study. Mice were injected with a single dose of 2×10^5 CFU *C. albicans* intravenously and/or with 20 mg DMI intraperitoneally daily for 4 days. At day 7, mice were infected with 5×10^6 CFU *S. aureus* intravenously, and survival was monitored for the following 7 days.

(B and C) Survival rate of mice in response to systemic *S. aureus* infection following administration of PBS, *C. albicans*, and/or DMI (n = 10) (PBS vs. DMI p = 0.067; PBS vs. *C. albicans* p = 0.067; *C. albicans* vs. DMI+*C. albicans* p = 0.068, log rank Mantel-Cox test).

(D) Schematic representation of the BCG vaccination study. Plasma was collected before vaccination, and peripheral blood mononuclear cells (PBMCs) were isolated before (day 0), 14 days, and 90 days after BCG vaccination. PBMCs were stimulated with *S. aureus* for 24 h, and secretion of pro-inflammatory cytokines was quantified.

(legend continued on next page)

trained immunity by BCG vaccination is associated with lower systemic inflammation,[43] and thus it is tempting to speculate that in an *in vivo* human BCG trained immunity context, higher ITA concentrations may be a predictor of individuals who will develop greater trained immunity features. However, it is important to highlight that the molecular effects of exogenous DMI human supplementation would possibly be distinct from endogenous ITA's properties and thus warrant further investigation.

In conclusion, we show that DMI-induced trained immunity is accomplished through transcriptomic and epigenomic reprogramming coupled with a high-energy metabolism, which ultimately allows for increased responsiveness. The potentiation of distinct metabolic pathways provides the building blocks and the signaling messengers that shape cellular responses. We have observed that trained immunity triggered by β-glucan[18] or BCG[39] is characterized by metabolic and transcriptional changes similar to DMI-trained macrophages, namely IFN responses and the glutathione synthesis pathway, which play a pivotal role in DMI trained immunity. We demonstrate that the immunomodulatory functions of ITA and its derivatives are of great complexity and are far from being fully understood. The mechanisms of action of DMI comprise and influence fundamental cellular processes, such as metabolism, epigenomics, and the redox state of the cell. These pathways are highly dynamic and can be differently modulated depending on the context, triggering both immune-enhancing and anti-inflammatory mechanisms. Further exploration of the molecular, metabolic, and epigenomic changes induced by ITA and derivatives in different cell types and disease models will be of great importance to fully assess the potential of the modulation of immune responses by this promising metabolite and open therapeutic avenue.

Limitations of the study

A quickly growing number of studies highlight the potential of ITA and its derivatives for the suppression of inflammation in different pathological contexts.[4,42] However, it is important to note that ITA and its derivatives do not produce similar biological responses. For example, unlike ITA, the synthetic ITA derivatives DMI and OI neither decreased SDH activity nor led to succinate accumulation.[37,44] Also, although OI and DMI decreased LPS-induced IFN-β secretion,[3] ITA boosted IFN-β secretion after LPS stimulation.[37] The endogenous form of ITA and its derivatives also trigger potentially distinct outcomes in sepsis. DMI treatment increased mice survival in an LPS-induced sepsis model,[45] while myeloid *IRG1* depletion increased mice survival in a polymicrobial sepsis model.[46] Here, we observed the disparity between ITA and DMI in the induced changes in metabolism and responsiveness. However, a limitation of our study is that we did not evaluate the possibility of itaconylation as a post-translational modification in the trained immunity setting.[3,28] Itaconylation of histones or enzymes may affect their function. This post-translational modification may account for the distinct mechanisms of action of DMI and

ITA and contribute to the molecular mechanism underlying DMI trained immunity, which remains to be fully determined. It is also important to highlight that our study was mainly performed in peripheral circulating monocytes, which might not recapitulate the responses of tissue-resident macrophages and other non-myeloid cells. Different resident cells may uptake, metabolize, and respond to DMI and ITA in distinct manners. Analyzing these cell- and tissue-specific differences would contribute to disentangling which clinically relevant disease models might benefit from the use of which ITA derivative.

STAR★METHODS

Detailed methods are provided in the online version of this paper and include the following:

- KEY RESOURCES TABLE
- RESOURCE AVAILABILITY
  - Lead contact
  - Materials availability
  - Data and code availability
- EXPERIMENTAL MODEL AND STUDY PARTICIPANT DETAILS
  - Animals
  - Human studies
  - Primary monocyte isolation and culture
- METHOD DETAILS
  - *In vitro* trained immunity model
  - Cytokine quantification
  - Chromatin immunoprecipitation (ChIP)
  - RNA sequencing
  - *In vitro* metabolomics
  - Seahorse XFb metabolic flux analysis
  - Glutathione, and ATP quantification
  - RNA isolation and RT-PCR
  - *In vivo* trained immunity model
  - Genetic analysis using *ex vivo* trained immunity responses of the BCG cohort
  - Metabolic analysis of the BCG cohort
  - Fungal killing capacity
  - Fungal phagocytosis
  - Total ROS production quantification
  - Mitochondrial membrane potential and mitochondrial ROS measurements
  - Chronic granulomatous disease (CGD) patient samples
- QUANTIFICATION AND STATISTICAL ANALYSIS

(E) Boxplots of SNPs around the *IRG1* gene (±500 kb) showing the fold change of IL-6, IL-1β, or IFNγ production by PBMCs after *in vivo* BCG vaccination and *ex vivo S. aureus* stimulation, in individuals stratified according to genotype. Direction and p value of the association adjusted for sex and age are presented in the table (n = 278).

(F) Scatterplot depicting the correlation between baseline ITA concentration in plasma and the fold change of IL-1β (n = 275) and TNF-α (n = 274) produced by PBMCs after *ex vivo* stimulation at 90 days compared with day 0.

AUTHOR CONTRIBUTIONS

A.V.F., S.K., V.A.C.M.K., W.J.H.K., F.L.v.d.V., M.G., B.N., and J.D.-A. conceived and designed the experiments. A.V.F., S.K., L.A.G., M.B., I.B., G.K., O.B., T.A., V.S., K.D.S., T.G., S.J.C.F.M., L.C.d.B., V.P.M., and G.R. performed the experiments. A.V.F., S.K., V.A.C.M.K., V.M., G.R., E.J.G.-B., and B.N. analyzed the results. A.V.F. wrote the manuscript. All authors critically read and edited the manuscript.

DECLARATION OF INTERESTS

REFERENCES

1. Michelucci, A., Cordes, T., Ghelfi, J., Pailot, A., Reiling, N., Goldmann, O., Binz, T., Wegner, A., Tallam, A., Rausell, A., et al. (2013). Immune-responsive gene 1 protein links metabolism to immunity by catalyzing itaconic acid production. Proc. Natl. Acad. Sci. USA *110*, 7820–7825. https://doi.org/10.1073/pnas.1218599110.

2. Lampropoulou, V., Sergushichev, A., Bambouskova, M., Nair, S., Vincent, E.E., Loginicheva, E., Cervantes-Barragan, L., Ma, X., Huang, S.C.C., Griss, T., et al. (2016). Itaconate links inhibition of succinate dehydrogenase with macrophage metabolic remodeling and regulation of inflammation. Cell Metab. *24*, 158–166. https://doi.org/10.1016/j.cmet.2016.06.004.

3. Mills, E.L., Ryan, D.G., Prag, H.A., Dikovskaya, D., Menon, D., Zaslona, Z., Jedrychowski, M.P., Costa, A.S.H., Higgins, M., Hams, E., et al. (2018). Itaconate is an anti-inflammatory metabolite that activates Nrf2 via alkylation of KEAP1. Nature *556*, 113–117. https://doi.org/10.1038/nature25986.

4. Bambouskova, M., Gorvel, L., Lampropoulou, V., Sergushichev, A., Loginicheva, E., Johnson, K., Korenfeld, D., Mathyer, M.E., Kim, H., Huang, L.H., et al. (2018). Electrophilic properties of itaconate and derivatives regulate the IκBζ-ATF3 inflammatory axis. Nature *556*, 501–504. https://doi.org/10.1038/s41586-018-0052-z.

5. Sakai, A., Kusumoto, A., Kiso, Y., and Furuya, E. (2004). Itaconate reduces visceral fat by inhibiting fructose 2,6-bisphosphate synthesis in rat liver. Nutrition *20*, 997–1002. https://doi.org/10.1016/J.NUT.2004.08.007.

6. Liao, S.T., Han, C., Xu, D.Q., Fu, X.W., Wang, J.S., and Kong, L.Y. (2019). 4-Octyl itaconate inhibits aerobic glycolysis by targeting GAPDH to exert anti-inflammatory effects. Nat. Commun. *10*, 5091. https://doi.org/10.1038/s41467-019-13078-5.

7. Nair, S., Huynh, J.P., Lampropoulou, V., Loginicheva, E., Esaulova, E., Gounder, A.P., Boon, A.C.M., Schwarzkopf, E.A., Bradstreet, T.R., Edelson, B.T., et al. (2018). Irg1 expression in myeloid cells prevents immuno-
pathology during M. tuberculosis infection. J. Exp. Med. *215*, 1035–1045. https://doi.org/10.1084/jem.20180118.

8. Muñoz-Elías, E.J., and McKinney, J.D. (2005). Mycobacterium tuberculosis isocitrate lyases 1 and 2 are jointly required for in vivo growth and virulence. Nat. Med. *11*, 638–644. https://doi.org/10.1038/nm1252.

9. Naujoks, J., Tabeling, C., Dill, B.D., Hoffmann, C., Brown, A.S., Kunze, M., Kempa, S., Peter, A., Mollenkopf, H.J., Dorhoi, A., et al. (2016). IFNs modify the proteome of legionella-containing vacuoles and restrict infection via IRG1-derived itaconic acid. PLoS Pathog. *12*, e1005408. https://doi.org/10.1371/journal.ppat.1005408.

10. Singh, S., Singh, P.K., Jha, A., Naik, P., Joseph, J., Giri, S., and Kumar, A. (2021). Integrative metabolomics and transcriptomics identifies itaconate as an adjunct therapy to treat ocular bacterial infection. Cell Rep. Med. *2*, 100277. https://doi.org/10.1016/J.XCRM.2021.100277.

11. Tomlinson, K.L., Lung, T.W.F., Dach, F., Annavajhala, M.K., Gabryszewski, S.J., Groves, R.A., Drikic, M., Francoeur, N.J., Sridhar, S.H., Smith, M.L., et al. (2021). Staphylococcus aureus induces an itaconate-dominated immunometabolic response that drives biofilm formation. Nat. Commun. *12*, 1399. https://doi.org/10.1038/s41467-021-21718-y.

12. Riquelme, S.A., Liimatta, K., Wong Fok Lung, T., Fields, B., Ahn, D., Chen, D., Lozano, C., Sáenz, Y., Uhlemann, A.-C., Kahl, B.C., et al. (2020). Pseudomonas aeruginosa utilizes host-derived itaconate to redirect its metabolism to promote biofilm formation. Cell Metab. *31*, 1091–1106.e6. https://doi.org/10.1016/j.cmet.2020.04.017.

13. Ferreira, A.V., Netea, M.G., and Domínguez-Andrés, J. (2019). Itaconate as an immune modulator. Aging *11*, 3898–3899. https://doi.org/10.18632/aging.102057.

14. Domínguez-Andrés, J., Novakovic, B., Li, Y., Scicluna, B.P., Gresnigt, M.S., Arts, R.J.W., Oosting, M., Moorlag, S.J.C.F.M., Groh, L.A., Zwaag, J., et al. (2019). The itaconate pathway is a central regulatory node linking innate immune tolerance and trained immunity. Cell Metab. *29*, 211–220.e5. https://doi.org/10.1016/J.CMET.2018.09.003.

15. Netea, M.G., Domínguez-Andrés, J., Barreiro, L.B., Chavakis, T., Divangahi, M., Fuchs, E., Joosten, L.A.B., van der Meer, J.W.M., Mhlanga, M.M., Mulder, W.J.M., et al. (2020). Defining trained immunity and its role in health and disease. Nat. Rev. Immunol., 1–14. https://doi.org/10.1038/s41577-020-0285-6.

16. Domínguez-Andrés, J., Arts, R.J.W., Bekkering, S., Bahrar, H., Blok, B.A., de Bree, L.C.J., Bruno, M., Bulut, Ö., Debisarun, P.A., Dijkstra, H., et al. (2021). In vitro induction of trained immunity in adherent human monocytes. STAR Protoc. *2*, 100365. https://doi.org/10.1016/j.xpro.2021.100365.

17. Kleinnijenhuis, J., Quintin, J., Preijers, F., Joosten, L.A.B., Ifrim, D.C., Saeed, S., Jacobs, C., van Loenhout, J., de Jong, D., Stunnenberg, H.G., et al. (2012). Bacille Calmette-Guerin induces NOD2-dependent nonspecific protection from reinfection via epigenetic reprogramming of monocytes. Proc. Natl. Acad. Sci. USA *109*, 17537–17542. https://doi.org/10.1073/pnas.1202870109.

18. Cheng, S.C., Quintin, J., Cramer, R.A., Shepardson, K.M., Saeed, S., Kumar, V., Giamarellos-Bourboulis, E.J., Martens, J.H.A., Rao, N.A., Aghajanirefah, A., et al. (2014). MTOR- and HIF-1α-mediated aerobic glycolysis as metabolic basis for trained immunity. Science *345*, 1250684. https://doi.org/10.1126/science.1250684.

19. Novakovic, B., Habibi, E., Wang, S.Y., Arts, R.J.W., Davar, R., Megchelenbrink, W., Kim, B., Kuznetsova, T., Kox, M., Zwaag, J., et al. (2016). β-Glucan reverses the epigenetic state of LPS-induced immunological tolerance. Cell *167*, 1354–1368.e14. https://doi.org/10.1016/j.cell.2016.09.034.

20. Arts, R.J.W., Moorlag, S.J.C.F.M., Novakovic, B., Li, Y., Wang, S.Y., Oosting, M., Kumar, V., Xavier, R.J., Wijmenga, C., Joosten, L.A.B., et al. (2018). BCG vaccination protects against experimental viral infection in humans through the induction of cytokines associated with trained immunity. Cell Host Microbe *23*, 89–100.e5. https://doi.org/10.1016/j.chom.2017.12.010.

21. Bannister, S., Kim, B., Domínguez-Andrés, J., Kilic, G., Ansell, B.R.E., Neeland, M.R., Moorlag, S.J.C.F.M., Matzaraki, V., Vlahos, A., Shepherd, R., et al. (2022). Neonatal BCG vaccination is associated with a long-term DNA methylation signature in circulating monocytes. Sci. Adv. 8, 4002. https://doi.org/10.1126/SCIADV.ABN4002.

22. Rinschen, M.M., Ivanisevic, J., Giera, M., and Siuzdak, G. (2019). Identification of bioactive metabolites using activity metabolomics. Nat. Rev. Mol. Cell Biol. 20, 353–367. https://doi.org/10.1038/s41580-019-0108-4.

23. Cordes, T., Wallace, M., Michelucci, A., Divakaruni, A.S., Sapcariu, S.C., Sousa, C., Koseki, H., Cabrales, P., Murphy, A.N., Hiller, K., et al. (2016). Immunoresponsive gene 1 and itaconate inhibit succinate dehydrogenase to modulate intracellular succinate levels. J. Biol. Chem. 291, 14274–14284. https://doi.org/10.1074/jbc.M115.685792.

24. Sohrabi, Y., Lagache, S.M.M., Schnack, L., Godfrey, R., Kahles, F., Bruemmer, D., Waltenberger, J., and Findeisen, H.M. (2018). mTOR-dependent oxidative stress regulates oxLDL-induced trained immunity in human monocytes. Front. Immunol. 9, 3155. https://doi.org/10.3389/fimmu.2018.03155.

25. Seger, R.A. (2019). Chronic granulomatous disease 2018: advances in pathophysiology and clinical management. LymphoSign J. 6, 1–16. https://doi.org/10.14785/lymphosign-2018-0012.

26. Quintin, J., Saeed, S., Martens, J.H.A., Giamarellos-Bourboulis, E.J., Ifrim, D.C., Logie, C., Jacobs, L., Jansen, T., Kullberg, B.J., Wijmenga, C., et al. (2012). Candida albicans infection affords protection against reinfection via functional reprogramming of monocytes. Cell Host Microbe 12, 223–232. https://doi.org/10.1016/j.chom.2012.06.006.

27. Kaufmann, E., Sanz, J., Dunn, J.L., Khan, N., Mendonça, L.E., Pacis, A., Tzelepis, F., Pernet, E., Dumaine, A., Grenier, J.-C., et al. (2018). BCG educates hematopoietic stem cells to generate protective innate immunity against Tuberculosis. Cell 172, 176–190.e19. https://doi.org/10.1016/j.cell.2017.12.031.

28. Qin, W., Qin, K., Zhang, Y., Jia, W., Chen, Y., Cheng, B., Peng, L., Chen, N., Liu, Y., Zhou, W., et al. (2019). S-glycosylation-based cysteine profiling reveals regulation of glycolysis by itaconate. Nat. Chem. Biol. 15, 983–991. https://doi.org/10.1038/s41589-019-0323-5.

29. Keating, S.T., Groh, L., van der Heijden, C.D.C.C., Rodriguez, H., Dos Santos, J.C., Fanucchi, S., Okabe, J., Kaipananickal, H., van Puffelen, J.H., Helder, L., et al. (2020). The Set7 lysine methyltransferase regulates plasticity in oxidative phosphorylation necessary for trained immunity induced by beta-glucan. Cell Rep. 31, 107548. https://doi.org/10.2139/ssrn.3444608.

30. Ferreira, A.V., Koeken, V.A.C.M., Matzaraki, V., Kostidis, S., Alarcon-Barrera, J.C., de Bree, L.C.J., Moorlag, S.J.C.F.M., Mourits, V.P., Novakovic, B., Giera, M.A., et al. (2021). Glutathione metabolism contributes to the induction of trained immunity. Cells 10, 971. https://doi.org/10.3390/cells10050971.

31. Cavalli, G., Tengesdal, I.W., Gresnigt, M., Nemkov, T., Arts, R.J.W., Domínguez-Andrés, J., Molteni, R., Stefanoni, D., Cantoni, E., Cassina, L., et al. (2021). The anti-inflammatory cytokine interleukin-37 is an inhibitor of trained immunity. Cell Rep. 35, 108955. https://doi.org/10.1016/j.celrep.2021.108955.

32. Li, Y., Zhang, P., Wang, C., Han, C., Meng, J., Liu, X., Xu, S., Li, N., Wang, Q., Shi, X., et al. (2013). Immune Responsive Gene 1 (IRG1) promotes endotoxin tolerance by increasing A20 expression in macrophages through reactive oxygen species. J. Biol. Chem. 288, 16225–16234. https://doi.org/10.1074/jbc.M113.454538.

33. Liu, X., Wu, X.-P., Zhu, X.-L., Li, T., and Liu, Y. (2017). IRG1 increases MHC class I level in macrophages through STAT-TAP1 axis depending on NADPH oxidase mediated reactive oxygen species. Int. Immunopharmacol. 48, 76–83. https://doi.org/10.1016/J.INTIMP.2017.04.012.

34. Hall, C.J., Boyle, R.H., Astin, J.W., Flores, M.V., Oehlers, S.H., Sanderson, L.E., Ellett, F., Lieschke, G.J., Crosier, K.E., and Crosier, P.S. (2013). Immunoresponsive gene 1 augments bactericidal activity of macrophage-lineage cells by regulating β-oxidation-dependent mitochondrial ROS pro-

35. Hall, C.J., Sanderson, L.E., Lawrence, L.M., Pool, B., van der Kroef, M., Ashimbayeva, E., Britto, D., Harper, J.L., Lieschke, G.J., Astin, J.W., et al. (2018). Blocking fatty acid–fueled mROS production within macrophages alleviates acute gouty inflammation. J. Clin. Invest. 128, 1752–1771. https://doi.org/10.1172/JCI94584.

36. Wagner, B.A., Buettner, G.R., and Burns, C.P. (1996). Vitamin E slows the rate of free radical-mediated lipid peroxidation in cells. Arch. Biochem. Biophys. 334, 261–267. https://doi.org/10.1006/abbi.1996.0454.

37. Swain, A., Bambouskova, M., Kim, H., Andhey, P.S., Duncan, D., Auclair, K., Chubukov, V., Simons, D.M., Roddy, T.P., Stewart, K.M., et al. (2020). Comparative evaluation of itaconate and its derivatives reveals divergent inflammasome and type I interferon regulation in macrophages. Nat. Metab. 2, 594–602. https://doi.org/10.1038/s42255-020-0210-0.

38. Saeed, S., Quintin, J., Kerstens, H.H.D., Rao, N.A., Aghajanirefah, A., Matarese, F., Cheng, S.-C., Ratter, J., Berentsen, K., van der Ent, M.A., et al. (2014). Epigenetic programming of monocyte-to-macrophage differentiation and trained immunity. Science 345, 1251086. https://doi.org/10.1126/science.1218595.

39. Arts, R.J.W., Carvalho, A., La Rocca, C., Palma, C., Rodrigues, F., Silvestre, R., Kleinnijenhuis, J., Lachmandas, E., Gonçalves, L.G., Belinha, A., et al. (2016). Immunometabolic pathways in BCG-induced trained immunity. Cell Rep. 17, 2562–2571. https://doi.org/10.1016/j.celrep.2016.11.011.

40. García-Giménez, J.L., Romá-Mateo, C., Pérez-Machado, G., Peiró-Chova, L., and Pallardó, F.V. (2017). Role of glutathione in the regulation of epigenetic mechanisms in disease. Free Radic. Biol. Med. 112, 36–48. https://doi.org/10.1016/j.freeradbiomed.2017.07.008.

41. Daly, R., Blackburn, G., Best, C., Goodyear, C.S., Mudaliar, M., Burgess, K., Stirling, A., Porter, D., McInnes, I.B., Barrett, M.P., et al. (2020). Changes in plasma itaconate elevation in early rheumatoid arthritis patients elucidates disease activity associated macrophage activation. Metabolites 10, 241. https://doi.org/10.3390/metabo10060241.

42. Ogger, P.P., Albers, G.J., Hewitt, R.J., O'Sullivan, B.J., Powell, J.E., Calamita, E., Ghai, P., Walker, S.A., McErlean, P., Saunders, P., et al. (2020). Itaconate controls the severity of pulmonary fibrosis. Sci. Immunol. 5, eabc1884. https://www.science.org/doi/10.1126/sciimmunol.abc1884.

43. Koeken, V.A., de Bree, L.C.J., Mourits, V.P., Moorlag, S.J., Walk, J., Cirovic, B., Arts, R.J., Jaeger, M., Dijkstra, H., Lemmers, H., et al. (2020). BCG vaccination in humans inhibits systemic inflammation in a sex-dependent manner. J. Clin. Invest. 130, 5591–5602. https://doi.org/10.1172/jci133935.

44. Nastasi, C., Willerlev-Olsen, A., Dalhoff, K., Ford, S.L., Gadsbøll, A.S.Ø., Buus, T.B., Gluud, M., Danielsen, M., Litman, T., Bonefeld, C.M., et al. (2021). Inhibition of succinate dehydrogenase activity impairs human T cell activation and function. Sci. Rep. 11, 1458. https://doi.org/10.1038/s41598-020-80933-7.

45. Zhang, S., Jiao, Y., Li, C., Liang, X., Jia, H., Nie, Z., and Zhang, Y. (2021). Dimethyl itaconate alleviates the inflammatory responses of macrophages in sepsis. Inflammation 44, 549–557. https://doi.org/10.1007/s10753-020-01352-4.

46. Wu, R., Liu, J., Wang, N., Zeng, L., Yu, C., Chen, F., Wang, H., Billiar, T.R., Jiang, J., Tang, D., et al. (2022). Aconitate decarboxylase 1 is a mediator of polymicrobial sepsis. Sci. Transl. Med. 14, eabo2028. https://doi.org/10.1126/scitranslmed.abo2028.

47. Moorlag, S.J., Matzaraki, V., Puffelen, J.H., Heijden, C., Keating, S., Groh, L., Röring, R.J., Bakker, O.B., Mourits, V.P., Koeken, V.A., et al. (2021). An integrative genomics approach identifies KDM4 as a modulator of trained immunity. Eur. J. Immunol. 52, 431–446. https://doi.org/10.1002/EJI.202149577.

48. Koeken, V.A.C.M., Qi, C., Mourits, V.P., de Bree, L.C.J., Moorlag, S.J.C.F.M., Sonawane, V., Lemmers, H., Dijkstra, H., Joosten, L.A.B., van Laarhoven, A., et al. (2022). Plasma metabolome predicts trained

duction. Cell Metab. 18, 265–278. https://doi.org/10.1016/J.CMET.2013.06.018.

immunity responses after antituberculosis BCG vaccination. PLoS Biol. *20*, e3001765. https://doi.org/10.1371/journal.pbio.3001765.

49. Langmead, B. (2010). Aligning short sequencing reads with Bowtie. Curr. Protoc. Bioinform. *Chapter 11*, Unit 11.7. https://doi.org/10.1002/0471250953.bi1107s32.

50. Turro, E., Su, S.Y., Gonçalves, Â., Coin, L.J.M., Richardson, S., and Lewin, A. (2011). Haplotype and isoform specific expression estimation using multi-mapping RNA-seq reads. Genome Biol. *12*, 1–15. https://doi.org/10.1186/GB-2011-12-2-R13/TABLES/3.

51. Heinz, S., Benner, C., Spann, N., Bertolino, E., Lin, Y.C., Laslo, P., Cheng, J.X., Murre, C., Singh, H., and Glass, C.K. (2010). Simple combinations of lineage-determining transcription factors prime cis-regulatory elements

required for macrophage and B cell identities. Mol. Cell *38*, 576–589. https://doi.org/10.1016/j.molcel.2010.05.004.

52. Kostidis, S., Addie, R.D., Morreau, H., Mayboroda, O.A., and Giera, M. (2017). Quantitative NMR analysis of intra- and extracellular metabolism of mammalian cells: a tutorial. Anal. Chim. Acta *980*, 1–24. https://doi.org/10.1016/J.ACA.2017.05.011.

53. Shabalin, A.A. (2012). Matrix eQTL: ultra fast eQTL analysis via large matrix operations. Bioinformatics *28*, 1353–1358. https://doi.org/10.1093/bioinformatics/bts163.

54. Fuhrer, T., Heer, D., Begemann, B., and Zamboni, N. (2011). High-throughput, accurate mass metabolome profiling of cellular extracts by flow injection-time-of-flight mass spectrometry. Anal. Chem. *83*, 7074–7080. https://doi.org/10.1021/ac201267k.

STAR★METHODS

KEY RESOURCES TABLE

REAGENT or RESOURCE	SOURCE	IDENTIFIER
Antibodies		
BV785 anti-human CD11b antibody (ICRF44)	Biolegend	Cat#301346; RRID AB_2563794
Anti-H3K4me3 (polyclonal)	Diagenode	Cat#C15410003; RRID:AB_2924768
Anti-H3K9me3 (polyclonal)	Diagenode	Cat#C15410193; RRID:AB_2616044
Bacterial and virus strains		
Candida albicans (UC820 strain)	ATCC	ATCC MYA-3573
Staphylococcus aureus (RN4220 strain)	[18]	N/A
Chemicals, peptides, and recombinant proteins		
Lipopolysaccharide from E. coli serotype 055:B5	Sigma-Aldrich	Cat#L2880
Pam3Cys	EMC Microcollections	Cat#L2000
Ficoll-Paque	GE Healthcare	Cat#17-1440-03
Percoll	Sigma-Aldrich	Cat#P1644
Protein A/G Magnetic beads	Diagenode	Cat#C03010021
β1,3-(D)glucan (β-glucan)	[38]	N/A
Dimethylitaconate	Sigma-Aldrich	Cat#592498
Itaconate	Sigma-Aldrich	Cat#I29204
4-octyl itaconate	[3]	N/A
Zymosan (from *S. cerevisiae*)	Sigma-Aldrich	Cat#Z4250
MTA	Sigma-Aldrich	Cat#D5011
Oligomycin A	Sigma-Aldrich	Cat#75351
FCCP	Sigma-Aldrich	Cat#C2920
Antimycin A	Sigma-Aldrich	Cat#A8674
Rotenone	Sigma-Aldrich	Cat#R8875
2-DG	Sigma-Aldrich	Cat#D6134
MitoTempo	Sigma-Aldrich	Cat#SML0737
TMRE	Sigma-Aldrich	Cat#87917
H2DCFDA	Life Technologies	Cat#D399
MitoSOX™ Red	Invitrogen	Cat#M36008
Zymosan (from S. cerevisiae)	Sigma-Aldrich	Cat#Z4250
Luminol	Sigma-Aldrich	Cat#A8511
DPI	Sigma-Aldrich	Cat#D2926
NAC	Sigma-Aldrich	Cat#A7250
AT	Sigma-Aldrich	Cat#T3251
BSO	Sigma-Aldrich	Cat#B2515
Glutathione Monoethyl Ester	Santa Cruz Biotechnology	Cat#sc-203974
TRIzol	Life Technologies	Cat#15596018
Power SYBR™ Green PCR Master Mix	Applied Biosystems	Cat#4368708
Critical commercial assays		
Human TNFα ELISA	R&D systems	Cat#DY210
Human IL-6 ELISA	R&D systems	Cat#DY206
Human IL-1β ELISA	R&D systems	Cat#DY201
Human IL-10 ELISA	R&D systems	Cat#DY217B
Human IL-1Ra ELISA	R&D systems	Cat#DY280

Continued

REAGENT or RESOURCE	SOURCE	IDENTIFIER
Human IFNγ ELISA	R&D systems	Cat#DY285B
pHrodo Green S. aureus BioParticles	ThermoFisher Scientific	Cat#P35382
iScript cDNA Synthesis Kit	Bio-Rad	Cat#1708891
GSH/GSSG ratio detection assay kit	Abcam	Cat#ab138881
ATP assay kit	Sigma-Aldrich	Cat#MAK190
Pan Monocyte Isolation Kit	Miltenyi	Cat#130-096-537
Pierce™ BCA Protein Assay Kit	ThermoFisher Scientific	Cat#23225
Deposited data		
RNA sequencing	This study	GEO: GSE212282
Experimental models: Organisms/strains		
Mouse: C57BL/6JOlaHsd	Hellenic Pasteur Institute, Athens, Greece	N/A
Human: primary monocytes from healthy volunteers	Sanquin Blood Bank	N/A
Human: primary monocytes from CGD patients and healthy volunteers	This study	N/A
Human: 300BCG cohort	[43,47,48]	N/A
Oligonucleotides		
Total of 26 oligonucleotides	Sigma-Aldrich	Table S1
Software and algorithms		
GraphPad Prism	Graphpad Software	https://www.graphpad.com
Kaluza 2.1	Beckman Coulter	https://www.beckman.com/flow-cytometry/software/kaluza
Bowtie	[49]	http://bowtie-bio.sourceforge.net/index.shtml
MMSEQ	[50]	https://github.com/eturro/mmseq
HOMER	[51]	http://homer.salk.edu/homer/motif
R (information on used packages available upon request)	N/A	https://www.r-project.org/about.html
Chenomx NMR suite 9.0	Chenomx	https://www.chenomx.com/

RESOURCE AVAILABILITY

Lead contact
Further information and requests for resources and reagents should be directed to and will be fulfilled by the lead contact, Jorge Domínguez-Andrés (jorge.dominguezandres@radboudumc.nl).

Materials availability
This study did not generate new unique reagents.

Data and code availability
RNA-seq data have been deposited at GEO and are publicly available as of the date of publication. Accession numbers are listed in the key resources table. This paper does not report original code. Any additional information required to reanalyze the data reported in this paper is available from the lead contact upon request.

EXPERIMENTAL MODEL AND STUDY PARTICIPANT DETAILS

Animals
Animal experiments were conducted in the Unit of Animals for Medical and Scientific purposes of the University General Hospital Attikon (Athens, Greece). All experiments were licensed from the Greek veterinary directorate under the protocol number 338087/27-05-2020. 40 C57BL/6JOlaHsd male mice (Hellenic Pasteur Institute) at 21–23 weeks old were used. Animals were housed in groups of 5 animals per enriched type-II cage on a 12 h light-dark diurnal cycle with room temperature between 21 and 23°C. Water and food were provided ad libitum. Mice were randomly stratified into experimental groups.

Human studies

In the BCG Cohort, healthy adults (n = 325) were included between April 2017 and June 2018 as part of the 300BCG study, which was approved by Arnhem-Nijmegen Medical Ethical Committee (NL58553.091.16) and performed as previously described.[43] Participants were vaccinated with a standard dose of 0.1mL BCG (Bulgaria strain, Intervax, Canada) intradermally in the left upper arm, and EDTA blood was collected before, 14 and 90 days after vaccination. At these three time points, 5×10^5 PBMCs were stimulated with 10^6 CFU/mL heat-killed *Staphylococcus aureus* at 37°C with 5% CO_2 for 24h. Production of IL-6, IL-1β and TNFα was measured after 24h, while IFNγ was measured after 7 days of stimulation, in supernatants. The fold change in cytokine production (after vaccination compared to baseline) was used as a measure of the trained immunity responses.

Primary monocyte isolation and culture

Buffy coats from healthy donors were obtained after written informed consent (Sanquin Blood Bank, Nijmegen, the Netherlands). Samples were anonymized to safeguard donor privacy. PBMC isolation was performed by differential density centrifugation over Ficoll-Paque (GE Healthcare). Subsequently, isolation of monocytes was performed with a hyper-osmotic Percoll (Sigma) density gradient centrifugation and washed once with pyrogen-free cold phosphate buffered saline (PBS). Cells were resuspended in RPMI medium Dutch modified (Invitrogen) supplemented with 5 μg/mL gentamicin (Centraform), 2mM Glutamax (Gibco), and 1mM pyruvate (Gibco). In order to ensure maximal purity, Percoll-isolated monocytes were left to adhere to polystyrene flat bottom plates (Corning) for 1h at 37°C 5% CO_2 and then washed once with warm PBS.

METHOD DETAILS

In vitro trained immunity model

10^5 monocytes were seeded on flat-bottom 96-well plates (Greiner) and incubated, in RPMI with 10% human pooled serum, with 5mM itaconate (ITA) (Sigma), 100μM 4-octyl itaconate (OI) (kindly provided by Richard C. Hartley, University of Glasgow, UK), 250μM dimethyl itaconate (Sigma), 1 or 2 μg/mL β-glucan for 24 h at 37C. β-1,3-(D)-glucan (β-glucan) from *Candida albicans* was kindly provided by Professor David Williams (College of Medicine, Johnson City, USA). In some experiments, 0.5mM 5′-deoxy-5′-methylthioadenosine (MTA) (Sigma), 0.5μM diphenyleneiodonium (DPI) (Sigma), 50μM a-tocopherol (AT) (Sigma), 1mM N-acetyl cysteine (NAC) (Sigma), 500μM MitoTempo (MT) (Sigma), 25μM DL-buthionine sulphoximine (BSO) (Sigma), 1mM 2-Deoxy-D-glucose (2-DG) (Sigma) or monoethyl ester GSH (EtGSH) (Santa Cruz Biotechnology) were added to the cells 1h prior to 250μM DMI. After 24h, conditioned media was collected, cells were washed once with warm PBS and left to differentiate in RPMI supplemented with 10% pooled human serum for 5 days, with one medium refreshment at day 3 of culture. At day 6, cells were restimulated with 10 ng/mL *Escherichia coli* lipopolysaccharide (LPS; serotype 055:B5, Sigma) in combination with 1μM oligomycin (Sigma) or 10 μg/mL Pam3Cys (EMC microcollections) when indicated for 24h.

Cytokine quantification

Cytokine production was determined using commercial ELISA kits IL-1β, IL-6, TNFα, IL-10, IL-1Ra and IFNγ (R&D Systems) following the instructions of the manufacturer.

Chromatin immunoprecipitation (ChIP)

Monocytes cultured for 6 days were fixed with 1% formaldehyde (Sigma) and sonicated. 1μg of fixed and sonicated chromatin was immunoprecipitated using 1μg of H3K4me3 or H3K9me3 Antibodies (Diagenode). Chromatin was purified with Qiaquick MinElute PCR purification Kit (Qiagen). Data was expressed as percentage of input samples. *IL6.1*, *IL6.2*, *TNFA.1* and *TNFA.2* primer pairs were employed for RT-PCR (Table S1).

RNA sequencing

Monocytes were isolated by negative selection (Pan Monocyte Isolation Kit, Miltenyi, purity higher than 90%), stimulated, and collected at various time points using TRIzol (Life Technologies) and stored at −80°C until required. Samples were submitted to Beijing Genomics Institute (BGI; Tai Po, Hong Kong), where RNA was isolated and sequenced. RNA integrity was evaluated with the Agilent 2100 system (Agilent Technologies). Strand specific RNA was sequenced on a DNBSEQ platform (paired-end, read length 150 pb) and at least 20 million clean reads were generated per sample. Data generated are available in GEO database under the accession number GEO: GSE212282. To quantify gene expression levels, raw fastq files reads were aligned to the hg19 human transcriptome using Bowtie.[49] Quantification of gene expression levels as total counts per transcript and Reads Per Kilobase Million (RPKM) was performed using MMSEQ.[50] Reads per transcript were normalized using DEseq2 and pairwise comparisons were performed for different stimulations, with differentially expressed genes (DEGs) designated as those that meet the following criteria: adjusted p value < 0.05 (Benjamini-Hochberg), fold change >2, and RPKM >5. Promoter transcription factor motif enrichment and overrepresented KEGG pathways were calculated using HOMER.[51] Heatmaps, bubble plots, and multidimensional scaling plots were generated using ggplot2 in R.

In vitro metabolomics

Monocytes were isolated negatively (Pan Monocyte Isolation Kit, Miltenyi, purity higher than 90%), stimulated, and collected at various time points. Sampling and nuclear magnetic resonance (NMR) metabolomic analysis was performed as described previously.[52] Briefly, cells were washed once with warm (37C) PBS and quenched with liquid nitrogen. Polar metabolites were extracted with a mixture of 6,75:0,75:2,5 (v/v/v) methanol/chloroform/water. Following centrifugation, the soluble polar extracts were collected and dried with nitrogen gas, while the pellets were stored for protein quantitation using the Pierce BCA Protein Assay Kit (ThermoFisher Scientific). Conditioned media were also collected, and extracellular metabolites were extracted with 100% LC-MS grade cold (−30C) methanol and dried with nitrogen gas. All dried extracts from cells and culture media were dissolved in 0.22 mL of 0.05 M phosphate buffer in 99.8% deuterated water for NMR. In all samples a known quantity of trimethylsilyl propionic-d4-sodium salt (TSP-d_4) was added to serve as reference and quantification standard. One NMR experiment (pulse sequence: *noesygppr1d*; Bruker Biospin Ltd) was collected for each sample in a 14.1 T (600 MHz for ^{1}H) Bruker Avance *Neo* NMR. All recorded NMR spectra were imported in Chenomx NMR suite 9.0 (Chenomx NMR suite, v9.0, Edmonton, AB, Canada) for the quantification of metabolites. Quantitative data (μM or nmoles) was then normalized to the protein weight of each sample.

Seahorse XFb metabolic flux analysis

For analysis of the 24h time point, 2×10^5 negatively isolated monocytes (Pan Monocyte Isolation Kit, Miltenyi) were seeded and stimulated directly in cartridges. For analysis after day 6 of culture, 10^7 monocytes were cultured in 10 cm Petri dishes (Greiner) and stimulated for 24h. At day 6 of culture, cells were detached with Versene solution (ThermoFisher Scientific), and 10^5 cells were seeded in cartridges. Analysis was performed in DMEM with 0.6mM glutamine, 5 mM glucose, and 1 mM pyruvate, pH 7.4. Cells were left to rest in a non-CO2-corrected incubator at 37ºC for 1h. Oxygen consumption rate (OCR) and extracellular acidification rate (ECAR) were measured using a Cell Mito Stress Kit in an XFp Analyzer (Seahorse Bioscience), with final concentrations of 1μM oligomycin (Sigma-Aldrich), 1μM FCCP (Sigma-Aldrich), and 0.5μM rotenone/antimycin A (Sigma-Aldrich). OCR measurements were used to calculate ATP production (basal OCR - OCR after oligomycin), H$^+$ leak (OCR after oligomycin – OCR after antimycin A/Rotenone), and spare respiratory capacity (SRC) (OCR after FCCP – basal OCR).

Glutathione, and ATP quantification

To determine intracellular glutathione concentration, 10^6 monocytes were lysed with 0.5% NP-40 in PBS at 5h of culture and samples were deproteinized with 100% TCA and neutralized with 0.5M NaHCO3, following the manufacturer instructions (Abcam). ATP levels were determined after macrophages were detached and incubated with or without 1μM oligomycin (Sigma-Aldrich) for 30min. The manufacturer's instructions were then followed (Sigma).

RNA isolation and RT-PCR

Total RNA was extracted by TRIzol (Life Technologies), according to the manufacturer's instructions, and quantified using a Nanodrop 2000 UV-visible spectrophotometer. cDNA was synthesized from 450ng to 1μg RNA by iScript Reverse Transcriptase (Bio-Rad). Relative expression was determined using SYBR Green (Applied Biosystems) on an Applied Biosciences StepOne PLUS RT-PCR machine. Fold changes in expression were calculated by the $\Delta\Delta$Ct method using HPRT1 as an endogenous control. The primer pairs used can be found in Table S1.

In vivo trained immunity model

Mice received a single intravenous injection of 2×10^5 live *C. albicans* blastoconidia (UC820 strain) or/and daily intraperitoneal injections of 10 mg DMI for 4 days. Pyrogen-free phosphate-buffered saline (PBS) injection was used as control alone. Seven days after the first injection, mice were infected intravenously with 5×10^6 cfu/mouse *Staphylococcus aureus*. Survival was monitored for 14 days.

Genetic analysis using *ex vivo* trained immunity responses of the BCG cohort

As previously described in,[47] DNA samples of individuals (n = 325) were genotyped using the commercially available SNP chip, Infinium Global Screening Array MD v1.0 from Illumina. Genotype information on approximately 4 million SNPs was obtained upon imputation (MAF> 5% and $R^2 > 0.3$ for imputation quality). Both genotype and cytokine data on trained immunity responses was obtained for a total of 296 individuals from the 300BCG cohort. Outliers were excluded and 278 samples were used for quantitative trait loci (QTL) mapping. Cytokine concentrations were log-transformed and the fold change of cytokine production (IL-6, IL-1β and IFNγ) between visits was mapped to genotype data using a linear regression model with age and sex as covariates. We used a cutoff of $p < 9,99 \times 10^{-3}$ to identify suggestive QTL associations affecting trained immunity responses. R-package Matrix-eQTL was used for cytokine QTL mapping.[53]

Metabolic analysis of the BCG cohort

As previously reported,[48] metabolite levels of the same individuals were measured in plasma collected prior to BCG vaccination. The metabolic features were measured and annotated by General Metabolics (Zurich, Switzerland) using flow injection time-of-flight mass (flow-injection TOF-M) spectrometry.[54] Non-targeted metabolites were annotated according to the human metabolites

database (HMDB). All metabolomic measurements were performed in duplicates, and the average value was calculated for each sample per metabolite. We performed a regression analysis corrected for age and sex between baseline levels of ITA and the fold change of *ex vivo* cytokine production.

Fungal killing capacity

10^5 monocytes were cultured for 24h and then infected with *C. albicans* conidia (UC820 (American Type Culture Collection MYA-3573)) for 3h in a multiplicity of inflection (MOI) of 2 at 37°C in RPMI 10% pooled human serum. Monocytes were then lysed with distilled water for 10min, and colony-forming units were assessed on Sabouraud agar plates. Killing capacity was expressed as a ratio to *C. albicans* cultured in the absence of cells.

Fungal phagocytosis

10^6 monocytes cultured for 24h and incubated with 0,15µL of pHrodo Green *S. aureus* BioParticles (ThermoFisher Scientific), followed by a quick spin. Cells were then incubated for 30 min at 4C and another 30 min at 37C. Analysis was performed in CytoFlex (Beckman Coulter) and using Kaluza 2.1 software (Beckman Coulter). Cell aggregates were gated out based on the forward scatter (FSC)-height versus FSC-area plot, monocytes/macrophages were gated according to a $CD11b^+$ (BV785, clone ICRF44, Biolegend) population.

Total ROS production quantification

Superoxide anion levels were evaluated using luminol-enhanced chemiluminescence and determined in a luminometer (Biotek Synergy HT). 10^5 monocytes were incubated with 250µM DMI, or RPMI alone for 1h followed by the addition of opsonized zymosan (1 mg/mL). Luminol (Sigma) was added to each well in order to start the chemiluminescence reaction. Each measurement was carried out in quadruplicates. Chemiluminescence was determined every 145 s at 37°C for 1h. Luminescence was expressed as relative light units (RLU) per second and as area under the curve (AUC). The fluorescent probe H2DCFDA was also used to determine reactive oxygen species levels. Monocytes/macrophages were cultured for 2h, 24h, or 6 days, washed, detached with cold PBS, and incubated with 5µM H2DCFDA (Life Technologies) in PBS for 30 min at 37°C. Cells were analyzed by flow cytometry (CytoFlex, Beckman Coulter).

Mitochondrial membrane potential and mitochondrial ROS measurements

Monocytes cultured for 24h or 6d were washed and detached with cold PBS. Approximately 5×10^5 cells were stained in 250µL of 5µM MitoSOX Red (Invitrogen) in HBSS 1mM Ca, 100nM tetramethylrhodamine ethyl ester perchlorate (TMRE, Sigma) in RPMI for 30 min at 37°C and 5% CO_2. Dyes allow for the evaluation of mitochondrial ROS production and mitochondrial membrane polarization, respectively. As a control, 10µM carbonyl cyanide p-trifluoro-methoxyphenyl hydrazone (FCCP) was added to TMRE stained cells. Cells were analyzed by flow cytometry (CytoFlex, Beckman Coulter).

Chronic granulomatous disease (CGD) patient samples

Blood was collected from age-matched healthy controls who did not suffer from infectious or inflammatory diseases and from CGD patients harboring homozygous mutations in the NCF1 gene (p47-phox) or X-linked mutation in CYBB gene (Gp91-phox), in which severely impaired ROS production has been demonstrated. All participants gave written informed consent. Inclusion of healthy controls was approved by the local institutional review board (CMO region Arnhem-Nijmegen, #2299 2010/104). According to the Dutch law, approval by an ethics committee was not required since the blood samples were part of regular clinical care. All experiments were performed and conducted in accordance with good clinical practice and the Declaration of Helsinki. PBMCs and monocytes were isolated and cultured as aforementioned.

QUANTIFICATION AND STATISTICAL ANALYSIS

For each experiment, sample size, number of replicates and associated statistical data can be found in figure legends. Data are presented as mean + SD, as indicated in the legend of each figure, unless otherwise stated. Data are judged to be statistically significant when $p < 0.05$, denoted by asterisks (*). For comparison between two groups, Wilcoxon signed rank test was performed; for comparison between more than two groups, one-way ANOVA followed by Dunnett's multiple comparisons test was used; for comparisons where we have two independent variables, two-way ANOVA followed by Sidak's multiple comparisons test was used. For the mice survival experiment, the Log rank Mantel-Cox test was performed. Significance evaluated by the above-mentioned tests were performed in Graphpad Prism (v6). QTL analysis and metabolic analysis of the BCG cohort was performed by a linear regression model with age and sex as covariates. Regarding generated RNA-sequencing data, reads per transcript were normalized using DEseq2 and pairwise comparisons were performed for different stimulations, with differentially expressed genes (DEGs) designated as those that meet the following criteria: adjusted p value < 0.05 (Benjamini-Hochberg), fold change >2, and RPKM >5. Promoter transcription factor motif enrichment and overrepresented KEGG pathways were calculated using HOMER.[51]